Optimal Postbuckling Design of Variable Angle Tow Composite Plates

Gangadharan Raju[1]
Indian Institute of Technology, Hyderabad 502285, India

Zhangming Wu[2]
Cardiff University, Wales, United Kingdom

Simon White[3]
University of Bristol, Bristol, England BS8 1TR, United Kingdom

Paul M Weaver[4]
University of Bristol, Bristol, England BS8 1TR, United Kingdom and

Bernal Institute, School of Engineering, University of Limerick, Ireland

Perturbation based approximation methods are widely used in preliminary design studies of thin-walled structures. In this work, postbuckling analysis of a variable angle tow (VAT) composite plate is performed using the perturbation-based asymptotic numerical method (ANM) which transforms the nonlinear problem into a set of well-posed recursive linear problems. These linear problems are solved using a novel generalized differential-integral quadrature method and the postbuckling solutions are sought over a finite load step size around the critical buckling point using asymptotic expansions. The accuracy of the ANM in evaluating the initial postbuckling of VAT plates under compression is investigated. Subsequently, a novel postbuckling optimization approach based on ANM results is proposed for design of VAT laminates. The postbuckling features obtained from ANM are used in an efficient two-level optimization framework

---

[1] Assistant Professor, Department of Mechanical and Aerospace Engineering
[2] Lecturer, Department of Mechanical and Aerospace Engineering
[3] PhD Student, Advanced Composite Centre for Innovation and Science, Department of Aerospace Engineering, Queen's Building, University Walk.
[4] Professor in Lightweight Structures, Advanced Composite Centre for Innovation and Science, Department of Aerospace Engineering, Queen's Building 2.39, University Walk. Member AIAA.

for design of VAT plates. At the first level, a globally convergent method of moving asymptotes is adopted to determine the optimal lamination parameter distributions that maximize the postbuckling performance of the VAT plate. At the second level, a genetic algorithm is used to convert the optimal lamination parameter distributions into realistic VAT layups. The optimization studies are performed for square VAT plates for axial/bi-axial compression under different in-plane boundary conditions.

Nomenclature

a,b,h	= Length, width and thickness of the plate (m)
u,v,w	= In-plane and Out-of-plane displacement field (m)
N_x, N_y	= Number of grid points along x, y directions
$\mathbf{T}^x$, $\mathbf{T}^y$	= First-order derivative matrix operators
$\mathbf{T}^{xx}$, $\mathbf{T}^{yy}$, $\mathbf{T}^{xy}$	= Second-order derivative matrix operators
$\mathbf{M}$	= Integral quadrature matrix operator over a surface area Ω
$\bar{N}_x, \bar{N}_y, \bar{N}_{xy}$	= In-plane stress resultants (N/m)
$N_m^{(k)}(\bar{u}), N_n^{(k)}(\bar{v})$	= B-spline basis functions varying along $\bar{u}$ and $\bar{v}$ directions
M_x, M_y, M_{xy}	= Moment resultants (N-m/m)
r	= Perturbation parameter
λ_c	= Critical buckling load (N)
P_{mn}	= Control points
$V(p), \bar{V}(p)$	= Mixed and pure displacement solutions of the p^{th} order problem
$C(p)$	= Postbuckling load coefficient of order p
K, K_g	= Structural and geometrical stiffness matrix of the plate structure
$\mathbf{A}, \mathbf{B}, \mathbf{D}$	= Laminate in-plane, coupling and bending stiffness matrices
$\Gamma_{0,1,2,3,4}$	= Matrices expressed as a function of material invariants
$\Gamma_{mn}^{(\tau)}$	= Lamination parameters at each pre-defined control point
μ, ν	= Indices of the outer and inner iterations
$\alpha_j^{(\mu)}, \beta_j^{(\mu)}$	= Upper and lower moving asymptotes
$\theta(\bar{z})$	= Layup angle as a function of normalized through-the-thickness coordinate
$\xi_{1,2,3,4}^A$	= In-plane lamination parameters
$\xi_{1,2,3,4}^B$	= Coupling lamination parameters
$\xi_{1,2,3,4}^D$	= Out-of-plane lamination parameters
ϵ_x	= Axial end-shortening strain
Ξ	= Knot vector

I. Introduction

Modern composite manufacturing technologies based on tow steering provide enhanced freedom to design efficient light-weight composite structures where stiffness varies continuously in the plane of each lamina. In the design process of thin and slender variable angle tow (VAT) panels, it can often be imperative to consider buckling as an important design constraint. Numerous works have been reported to maximize the buckling performance of VAT laminates [1–3]. Interestingly, the optimal stiffness distributions for maximizing buckling eigenvalues oppose that for maximizing postbuckling axial stiffness (chapter 6 by Weaver in Ref. 4). Whilst buckling performance is a function of bending stiffness, postbuckling behavior is a function of membrane stiffness of the composite panel. Therefore, it is necessary to improve both the buckling and postbuckling performance for a better structural response.

In the current design philosophy the operating limit load for primary aircraft structures can be driven by buckling load. It is known that plate-like structures can carry loads in to the post-buckling region without material failure. New design philosophies allow the operating load limit to extend into the postbuckling regime that enables reduction of weight of laminated composite structures. Thus, we need tools to accurately simulate the structural behavior in the postbuckling regime. Incremental finite element models are a reliable option for studying postbuckling response, however computational effort required is significant and not necessarily appropriate for optimization studies. Therefore, new numerical tools which are quick and reasonably accurate for studying the postbuckling response of VAT laminates are required in initial design studies.

Much work has been reported on semi-analytical modeling methods for studying the postbuckling behavior of structures. Stein [5] proposed a perturbation approach to model the initial postbuckling behavior of isotropic plates under different in-plane boundary conditions. Later, Chandra and Raju [6] extended Stein's approach for an orthotropic plate. Harris [7] developed a closed-form expression to determine the initial postbuckling stiffness of orthotropic composite plates. Pandey and Sherbourne [8] derived expressions for initial postbuckling stiffness of composite plates and used them for optimization studies. Zhang and Shen [9] employed the perturbation approach similar to Stein [5], but employed Airy's stress function to derive the closed-form asymptotic postbuckling

solutions for plates under axial and biaxial compression. Recently, Wu et al. [10] enhanced Zhang and Shen's work for composite plates and derived explicit closed-form expressions for both the end shortening strain and maximum transverse deflection as a function of material stiffness and stress resultants. The improved accuracy of their postbuckling solution is mainly due to the selection of perturbation parameter based on in-plane stress resultant instead of maximum transverse displacement. Rahman et al. [11] used a finite element perturbation approach to study the postbuckling behavior of VAT plates. In their approach, the postbuckling solutions were computed by expanding the load and displacement fields around the buckling load up to second order fields. This approach resulted in reasonably accurate solutions very close to the buckling point and exhibits erroneous solutions for a finite load step in the postbuckling regime for straight fiber as well as VAT plates. This problem can be overcome by including higher order asymptotic fields in evaluating the postbuckling response of VAT plates. Damil and Potier-Ferry [12] proposed an asymptotic numerical method (ANM) which is a combination of a perturbation technique and a finite element method to solve the postbuckling problem of elastic structures. ANM transforms the nonlinear problem into a set of well-posed recursive linear problems solved using finite element method. ANM allows a generic approach to compute the higher order asymptotic solutions up to any order and provides reasonably accurate initial postbuckling solution. Azrar et al. [13] applied ANM to compute the postbuckling behavior of elastic plates and shells. Cochelin et al. [14] used ANM along with Padé approximants to improve the range of convergence of the postbuckling solution of plate and shell structures. In this work, the ANM approach is used to solve the postbuckling problem of VAT laminates under compression loading. A novel generalized differential-integral quadrature method is used instead of finite element method to solve the recursive set of linear problems obtained using ANM.

The design and optimization problem of VAT composite laminates poses many difficulties in terms of the non-convexity of the objective function, the number of design variables and the manufacturing constraints of tow placement. Ghiasi et al. [15] discussed various optimization methods and their essence in solving the design optimization problem of VAT laminates. Wu et al. [16] employed a genetic algorithm to determine the optimal VAT configuration for maximizing the postbuckling performance. Henrichsen et al. [17] used Koiter's asymptotic method along with continuous

fiber angle optimization for optimizing the postbuckling performance of VAT plates. Diaconu and Weaver [18, 19] employed a two-level optimization strategy for the postbuckling design of long symmetrical and unsymmetrical composite plates. Wu et al. [20] extended the two-level optimization framework to design VAT laminates with improved buckling performance. In this work, the two-level optimization strategy is adopted to design VAT laminates for maximizing their postbuckling performance.

The main objective of this paper is to extract postbuckling parameters of composite plates using ANM and subsequently use them as input to an optimization framework for design of VAT laminates. At the first step, the nonlinear postbuckling problem of VAT plates is converted into a set of linear problems using ANM. The resulting linear problems are solved using the generalized differential-integral quadrature method (GDIQM). Usage of GDIQM enables the C1 continuity requirements of a Kirchhoff-Love plate to be modeled more simply than with finite element methods. The numerical implementation of the GDIQM is done in a MATLAB software environment to compute the initial postbuckling solution of VAT plates. Padé approximants are then used to expand the ANM perturbed solutions so as to increase the range of validity of the postbuckling solution around the buckling point. The accuracy and the range of validity of the initial postbuckling solution computed using ANM for simply supported symmetric VAT plates under compression is investigated for different in-plane boundary conditions. Next, a two-level optimization strategy is used for maximizing the postbuckling performance of VAT laminates based on ANM results. In the first optimization level, lamination parameters are used as design variables to perform the postbuckling optimization. In this work, the optimization study is restricted to orthotropic VAT laminates which are defined using four lamination parameters ($\xi_{1,2}^{A,D}$). B-splines are used to define the lamination parameter distribution over the domain of the plate and the distributions are specified using a set of control points and a knot vector. The lamination parameters are not independent and are connected by a set of nonlinear constraints to define the feasible region [21]. The nonlinear constraints of the lamination parameters were enforced on the control points by employing the convex-hull property of the B-splines [20]. The gradient-based, globally convergent method of moving asymptotes is adopted to determine the optimal lamination parameter distributions of the VAT plate. In the

second optimization level, a genetic algorithm converts the optimal lamination parameters into realistic VAT layups. The postbuckling optimization studies are carried out for simply supported square VAT plates under axial/bi-axial compression for different in-plane boundary conditions.

The paper is organized as follows. In Section 2, the formulation of the ANM approach in solving the postbuckling of VAT plates is presented. Section 3 presents the numerical implementation of the generalized differential-integral quadrature method to perform postbuckling analysis of VAT laminates. In Section 4, the lamination parameters and the nonlinear constraints that governs their feasible region is presented. In Section 5, the two-level optimization framework employed for design of VAT laminates including globally convergent method of moving asymptote and genetic algorithm is discussed. Section 6 presents the optimization results of VAT laminates for maximizing the postbuckling performance is presented.

II. Asymptotic Numerical Method

The postbuckling problem of elastic structures is usually solved using a predictor-corrector algorithm based on the Newton-Raphson method or the Riks arc-length method. This approach can be successful in solving the nonlinear problem, but its main limitation is the high computational time involved, which makes it unsuitable for optimization studies. An alternative approach is to rely on perturbation methods for solving the postbuckling problem, which provide accurate solutions near the buckling load and requires less computational effort. In Koiter's perturbation method [23, 24], the displacement and loads are expanded up to second order displacement fields which provide qualitative results describing the postbuckling stability and imperfection sensitivity of the structure. The postbuckling solutions based on Koiter's approach are valid near the buckling point and are not reliable remote from it. The range of validity of Koiter's approach around the buckling point can be increased by considering cubic and higher order displacement fields. In the present work, the nonlinear postbuckling problem of VAT laminate is solved using a perturbation approach termed the asymptotic numerical method (ANM) proposed by Damil and Potier-Ferry [12]. The ANM solution is sought by means of considering asymptotic expansions higher than second order displacement fields for better accuracy and wider range of validity. In the ANM approach, the nonlinear problem

is converted into a series of well-posed recurrent linear problems by using asymptotic expansions of the displacement and stress resultant fields about the critical buckling load [13, 14].

In symmetric VAT panels, stiffness (A, D matrices) varies with $x-y$ coordinates and the constitutive equation in partial inverse form is given by,

$$\begin{Bmatrix} \epsilon \\ \bar{M} \end{Bmatrix} = \begin{bmatrix} A^*(x,y) & 0 \\ 0 & D(x,y) \end{bmatrix} \begin{Bmatrix} \bar{N} \\ \kappa \end{Bmatrix} \tag{1}$$

where $\bar{N}, \bar{M}$ are the stress and moment resultants, $A^* = A^{-1}$ is the compliance matrix and D is the bending stiffness matrix. Based on Kirchhoff-Love plate theory, the nonlinear mid-plane strains ϵ and curvatures κ are defined as

$$\begin{aligned} &\epsilon = \epsilon^L + \epsilon^{NL}, \\ &\epsilon^L = \begin{Bmatrix} u_{,x} \\ u_{,y} \\ u_{,y} + v_{,x} \end{Bmatrix}, \quad \epsilon^{NL} = \begin{Bmatrix} \frac{1}{2} w_{,x}^2 \\ \frac{1}{2} w_{,y}^2 \\ w_{,x} w_{,y} \end{Bmatrix} \\ &\kappa = \begin{Bmatrix} -w_{,xx} \\ -w_{,yy} \\ -2w_{,xy} \end{Bmatrix} \end{aligned} \tag{2}$$

where u, v, w are the displacements. The Hellinger-Reissner [25] mixed variational energy form of the plate is used for asymptotic expansions and is given by

$$\mathcal{L}\left(U_\alpha, W, \bar{N}\right) = \int_\Omega \epsilon : \bar{N} - \frac{1}{2} \bar{N} : A^* : \bar{N} + \frac{1}{2} \kappa : D : \kappa \quad d\Omega - \lambda \mathcal{P}\left(U_\alpha, W\right) \tag{3}$$

where $U_\alpha = \{u, v\}$ are the in-plane displacements, $W = \{w\}$ is the out-of-plane displacement in the transverse direction and $A : B$ represent the inner product of tensors (A, B). Defining the mixed unknown vector

$$U = \begin{Bmatrix} U_\alpha \\ W \\ \bar{N} \end{Bmatrix},$$

the governing equation of the model can be obtained by taking variation of the energy functional

Eqn. 3 with respect to U and is given by,

$$\begin{aligned} &\delta\left(\mathcal{L}\left(U\right)\right)=0, \quad \forall\delta U, \\ &\langle\langle L(U),\delta U\rangle\rangle+\left(\lambda-\lambda_c\right)\langle\langle L'(U),\delta U\rangle\rangle+\langle\langle Q(U,U),\delta U\rangle\rangle=0 \quad \forall\delta U, \end{aligned} \tag{4}$$

where λ_c is the critical buckling load, $\langle\langle .,. \rangle\rangle$ is a scalar product, $\langle\langle L(U),\delta U\rangle\rangle$, $\langle\langle L'(U),\delta U\rangle\rangle$ are linear operators and $\langle\langle Q(U,U),\delta U\rangle\rangle$ is a bi-linear operator. The operators in Eqn. 4 are expressed as

$$\begin{aligned} \langle\langle L(U),\delta U\rangle\rangle &= \int_\Omega \bar{N}:\delta\epsilon^L+(\epsilon^L-A^*:\bar{N}):\delta\bar{N}+\kappa:D:\delta\kappa d\Omega+\lambda_c\int_\Omega \bar{N}^0:\delta\epsilon^{NL}d\Omega, \\ \langle\langle L'(U),\delta U\rangle\rangle &= \int_\Omega \bar{N}^0:\delta\epsilon^{NL}d\Omega, \\ \langle\langle Q(U,U),\delta U\rangle\rangle &= \int_\Omega \epsilon^{NL}:\delta\bar{N}+\bar{N}:\delta\epsilon^{NL}d\Omega \end{aligned} \tag{5}$$

Using the implicit function theorem, the unknown U and the load parameter λ can be expanded into a series in parameter r,

$$\begin{aligned} \lambda-\lambda_c &= \sum_{p=1}^{\infty} C\left(p\right)r^p, \\ U &= U_0+\sum_{p=1}^{\infty} r^p V\left(p\right) \end{aligned} \tag{6}$$

with $V(p)$ orthogonal to $V(1)$ for $p\geq 2$,

$$\langle\langle V(p),V(1)\rangle\rangle=0, \quad p\geq 2 \tag{7}$$

The principle of ANM is to compute successively a number of vectors $V(p)$ and coefficients $C(p)$ up to a given order n. The polynomials $\lambda(r,n), U(r,n)$ are approximations of the exact solution branch. Substitution of Eqn. 6 into Eqn. 5 results in a set of linear problems in $V(p), C(p)$ given by

$$\begin{aligned} &\langle\langle L(V(p)),\delta U\rangle\rangle=\langle\langle F(p),\delta U\rangle\rangle \quad \forall\delta U \\ &\langle\langle L(V(p)),V(1)\rangle\rangle=0 \\ &C(p-1)=\tfrac{1}{\langle\langle L'(V(1)),V(1)\rangle\rangle}\times\left[-\sum_{k=1}^{p-2}C(k)\langle\langle L'(V(p-k)),V(1)\rangle\rangle-\sum_{k=1}^{p-1}\langle\langle Q(V(k),V(p-k)),V(1)\rangle\rangle\right] \end{aligned} \tag{8}$$

The force term $F(p)$ is defined as

$$\begin{aligned} \langle\langle F(p),\delta U\rangle\rangle &= \int_\Omega F^U_\alpha(p)\delta W_{,\alpha}+F^{\bar{N}}_{\alpha\beta}(p)\delta\bar{N}_{,\alpha\beta}d\Omega \\ F^U_\alpha(p) &= -\sum_{k=1}^{p-1}(C(r)\bar{N}^0_{\alpha\beta}+\bar{N}^k_{\alpha\beta})W_{,\beta}(p-k) \\ F^{\bar{N}}_{\alpha\beta}(p) &= -\sum_{k=1}^{p-1}\tfrac{1}{2}W_{,\alpha}(k)W_{,\beta}(p-k) \end{aligned} \tag{9}$$

The next step is to convert the linear mixed variable problem given by Eqns. 8, 9 into linear displacement problems and the details of the conversion are given in the work by Azrar et al. [13]. For flat plate-like structures loaded by in-plane forces, the fundamental solution is a pure in-plane elasticity problem with no transverse deflections. The first bifurcation is symmetric and the associated problem is a pure bending deformation. For plates, Eqn. 6 can be simplified into

$$\begin{aligned} &\lambda - \lambda_c = C(2)r^2 + C(4)r^4 + C(6)r^6 + ... \\ &U - U_0 = r\begin{Bmatrix} 0 \\ W(1) \\ 0 \end{Bmatrix} + r^2\begin{Bmatrix} U_\alpha(2) \\ 0 \\ \bar{N}_{\alpha\beta}(2) \end{Bmatrix} + r^3\begin{Bmatrix} 0 \\ W(3) \\ 0 \end{Bmatrix} + r^4\begin{Bmatrix} U_\alpha(4) \\ 0 \\ \bar{N}_{\alpha\beta}(4) \end{Bmatrix} + ... \end{aligned} \tag{10}$$

where r is the perturbation parameter. The coefficients $C(p)$ are zero when p is odd. Similarly, $V(p)$ is in-plane displacement when p is even and out-of-plane displacement if p is odd. The ANM solution given by Eqn. 10 coincides with the exact solution for small values of the parameter r because the terms r^n are close to zero for $r < 1$. But beyond a critical point $r > 1$, the terms r^n grow rapidly and the ANM solution starts to diverge. This problem is overcome by using Padé approximation[14] to define the displacement and load fields given by,

$$\begin{aligned} \lambda - \lambda_c &= \sum_{k=1}^{n} f_k(r) C_k \\ U - U_0 &= \sum_{k=1}^{n} f_k(r) U_k \\ f_k &= \tfrac{P_k(r)}{Q_k(r)} \end{aligned} \tag{11}$$

where f_k are the Padé approximants. Therefore, usage of Padé approximation in the asymptotic expansions increases the radius of convergence of ANM solutions when compared to using polynomial expansions. The set of linear displacement problems in Eqn. 9 are solved using a generalized differential-integral quadrature method explained in the next section.

III. Generalized differential-integral quadrature method

Differential quadrature method (DQM) has been successfully applied to solve the partial differential equations that governs the buckling and postbuckling behavior of VAT laminates [26, 27]. The DQM approach is based on the approximation of a derivative using a weighted linear sum of the function values at discretised grid points in the domain. In this work, the generalised differential-

integral quadrature method (GDIQM) is applied to solve different order linear variational integral expressions of the postbuckling problem obtained from the ANM approach. The differential and integral operators present in the linear problems (Eqn. 11) are approximated using weighting matrices and solved for the unknowns $\bar{V}(p), C(p)$. The GDIQM advances on the quadrature rule proposed by Shu et al. [28, 29]. White et al. [30] introduced the GDIQM approach to solve the integro-differential postbuckling equations of VAT laminates derived using Koiter's approach. The postbuckling response of laminates were limited to the quadratic expansion displacement fields and resulted in good agreement in the vicinity of the buckling point. In current work, as a novelty, GDIQM is used to solve a set of linear problems (Eqn. 9) obtained using ANM for computing the postbuckling response over a finite load step around the buckling point.

A. Differentiation weighting matrix

Assume that both the independent variables (x, y) and dependent variables $F(x, y)$ have been discretised and assembled into a grid $(x, y)_i$ and F_i respectively, where i is the nodal index ranges between $i = 1..N_xN_y$. The terms N_x, N_y represent the number of grid points along x and y directions. The standard generalized differential quadrature [28] equation is,

$$\frac{\partial F_i}{\partial x} = \sum_{i=1}^{N_xN_y} T^x_{ik} F_k \quad \text{with} \quad k = 1..N_xN_y \tag{12}$$

where T^x_{ik} represents the weighting coefficient matrix of the first order derivative. Making the grid-point variables, F_i, the components of the vector $\mathbf{F}$, the first-order partial derivative is written in matrix form as,

$$\frac{\partial}{\partial x}\mathbf{F} = \mathbf{T}^x\mathbf{F}, \quad \frac{\partial}{\partial y}\mathbf{F} = \mathbf{T}^y\mathbf{F}, \tag{13}$$

where $\mathbf{T}^x, \mathbf{T}^y$ are the first-order derivative matrix operators along x and y directions. Similarly, we can define second-order partial derivatives as,

$$\frac{\partial^2}{\partial x^2}\mathbf{F} = \mathbf{T}^{xx}\mathbf{F}, \quad \frac{\partial^2}{\partial y^2}\mathbf{F} = \mathbf{T}^{yy}\mathbf{F}, \quad \frac{\partial^2}{\partial x \partial y}\mathbf{F} = \mathbf{T}^{xy}\mathbf{F} \tag{14}$$

where $\mathbf{T}^{xx}, \mathbf{T}^{yy}, \mathbf{T}^{xy}$ are the second-order derivative matrix operators.

B. Integration weighting matrix

Given a simple 1D function $f(x)$, indefinite integration weighting coefficients for an arbitrary grid spacing can be calculated using the Moore-Penrose pseudo inverse operation [31]. This is written as

$$\left(\int f \,\mathrm{d}x\right)_i \approx j^x_{ik} f_k + c \quad \text{with} \quad \mathbf{j}^x = (\mathbf{T}^x)^+ \,;\, i,k = 1..N \tag{15}$$

where c is a constant of integration and $()^+$ is the Moore-Penrose pseudo inverse operation. Eqn 15 is used to calculate weighting coefficients for definite integration. These are calculated by simply subtracting the numerical value of the indefinite integrals at $i = 1$ and N. Hence:

$$\int_0^{l_x} f \,\mathrm{d}x \approx w^x_k f_k \quad \text{with} \quad w^x_k = j^x_{Nk} - j^x_{1k} \tag{16}$$

where w^x_k are the elements of the integration vector $\mathbf{w}^x$. In the two-dimensional case eqn. 16 is written:

$$\int_0^{l_x}\int_0^{l_y} F(x,y)\; \mathrm{d}x\mathrm{d}y \approx \mathbf{w}^{xy}\mathbf{F} \tag{17}$$

The vector $\mathbf{w}^{xy}$ is assembled for a particular grid-point numbering scheme using eqns. 15 and 16.

The integral of a product of two functions $F(x,y)$ and $G(x,y)$ can be calculated approximately by constructing a matrix, $\mathbf{M} = \mathrm{diag}(\mathbf{w}^{xy})$, such that

$$\int_0^{l_x}\int_0^{l_y} F(x,y)\, G(x,y)\; \mathrm{d}x\mathrm{d}y \approx \mathbf{F}^T\mathbf{M}\mathbf{G}$$

where $\mathbf{M}$ is the integral quadrature matrix operator acting on a function defined over a surface area Ω

C. Computation of $\bar{V}(p)$ and $C(p)$ using GDIQM

Applying GDIQM to Eqn. 9 then,

$$[K - \lambda_c K_g]\bar{V}(p) = [\bar{F}(p)] \tag{18}$$

where $[K]$ is the stiffness matrix of the plate structure, $[K_g]$ is the geometric stiffness of the structure and $\bar{V}(p)$ is the solution of the p^{th} order problem. In addition, the orthogonality condition between

$\bar{V}(p)$ and $\bar{V}(1)$ should be added to obtain a unique solution. This condition is enforced using a Lagrange multiplier approach given by

$$\begin{bmatrix} K - \lambda_c K_g & \bar{G}^* \\ \bar{G}^{*t} & 0 \end{bmatrix} \begin{Bmatrix} \bar{V}(p) \\ \mu \end{Bmatrix} = \begin{Bmatrix} \bar{F}(p) \\ 0 \end{Bmatrix} \tag{19}$$

where μ is the Lagrange multiplier and $\bar{G}^* = [K]\bar{V}_1$. The solutions $\bar{V}(p)$ was then used to evaluate the postbuckling coefficients $C(p)$. The generality of GDIQM when compared with DQM allows different types of boundary conditions to be implemented effectively with less numerical effort. The postbuckling problem of VAT laminates under different in-plane boundary conditions is studied using GDIQM and the equations are given in the Appendix.

IV. Lamination Parameters

The stiffness matrices $\mathbf{A}(\mathbf{x},\mathbf{y}), \mathbf{B}(\mathbf{x},\mathbf{y})$ and $\mathbf{D}(\mathbf{x},\mathbf{y})$ are expressed as a linear combination of lamination parameters and material invariants [32]. In the present study, only specially orthotropic VAT laminates are considered. In other words, there is no in-plane and out-of-plane coupling ($\mathbf{B} = 0$), no shear-extension coupling ($A_{16} = 0, A_{26} = 0$) and no flexural-twisting coupling ($D_{16} = 0, D_{26} = 0$). As a result, two in-plane and two out-of-plane lamination parameters are sufficient to define the stiffness matrices as,

$$\begin{Bmatrix} A_{11} \\ A_{22} \\ A_{12} \\ A_{66} \end{Bmatrix} = h \begin{bmatrix} 1 & \xi_1^A & \xi_2^A & 0 & 0 \\ 1 & -\xi_1^A & \xi_2^A & 0 & 0 \\ 0 & 0 & -\xi_2^A & 1 & 0 \\ 0 & 0 & -\xi_2^A & 0 & 1 \end{bmatrix} \begin{Bmatrix} U_1 \\ U_2 \\ U_3 \\ U_4 \\ U_5 \end{Bmatrix} \tag{20}$$

$$\begin{Bmatrix} D_{11} \\ D_{22} \\ D_{12} \\ D_{66} \end{Bmatrix} = \frac{h^3}{12} \begin{bmatrix} 1 & \xi_1^D & \xi_2^D & 0 & 0 \\ 1 & -\xi_1^D & \xi_2^D & 0 & 0 \\ 0 & 0 & -\xi_2^D & 1 & 0 \\ 0 & 0 & -\xi_2^D & 0 & 1 \end{bmatrix} \begin{Bmatrix} U_1 \\ U_2 \\ U_3 \\ U_4 \\ U_5 \end{Bmatrix} \tag{21}$$

where U_1, U_2, U_3, U_4, U_5 are material invariants [33]. The four lamination parameters are defined by,

$$\begin{aligned} \xi_{1,2}^{A} &= \int_{-1}^{1} [\cos(2\theta(\bar{z}))\cos(4\theta(\bar{z}))]\, d\bar{z} \\ \xi_{1,2}^{D} &= \frac{3}{2}\int_{-1}^{1} [\cos(2\theta(\bar{z}))\cos(4\theta(\bar{z}))]\, d\bar{z} \end{aligned} \tag{22}$$

where $\theta(\bar{z})$ is the layup function in the thickness direction of the plate.

A. Feasible Region of Lamination Parameters

For variable angle tow (VAT) composites, lamination parameters are continuously varying with respect to the x and y coordinates. The corresponding nonlinear constraints for lamination parameters should be satisfied for all x, y. By not satisfying the constraints either gives rise to an unstable optimization process or could result in a physically infeasible optimal lamination configuration. Hence, an accurate boundary definition of the feasible region of lamination parameters is vital to the optimization of VAT laminates. The feasible region of the four lamination parameters ($\xi_{1,2}^{A,D}$) are well-bounded by a set of closed-form expressions [22], which are derived from Bloomfield et al.'s [34] and Wu et al.'s work [20],

$$5(\xi_1^A - \xi_1^D)^2 - 2(1 + \xi_2^A - 2(\xi_1^A)^2) \leq 0 \tag{23}$$

$$(\xi_2^A - 4t\xi_1^A + 1 + 2t^2)^3 - 4(1 + 2|t| + t^2)^2(\xi_2^D - 4t\xi_1^D + 1 + 2t^2) \leq 0 \tag{24}$$

$$(4t\xi_1^A - \xi_2^A + 1 + 4|t|)^3 - 4(1 + 2|t| + t^2)^2(4t\xi_1^D - \xi_2^D + 1 + 4|t|) \leq 0 \tag{25}$$

where $t = [-1, -0.8, -0.6, -0.4, -0.2, 0, 0.2, 0.4, 0.6, 0.8, 1]$. These 23 equations in Eqns. 23-25 are able to bound the feasible region of the four lamination parameters ($\xi_{1,2}^{A,D}$) with reasonably good accuracy. Hence, our approach requires much less computational effort in a optimization process than the convex hull approach [35], which employs $37,126$ linear equations to approximately bound the feasible region.

V. Optimization framework for design of VAT panels

The design of VAT panels is a challenging task as one has to determine the optimal layup at each x, y cooordinate of the plate. The postbuckling design criteria of VAT composite plates are based on the minimization of the end shortening strain ϵ_x or the maximum postbuckling transverse displacement W_{max} for a given compressive load.

A. First-Level Optimization

1. *B-spline spatial variation of lamination parameters*

In the case of a symmetric VAT plate, the distribution of lamination parameters ($\xi_{1,2}^{A,D}$) in terms of the B-spline is given as,

$$\begin{aligned} x(\bar{u},\bar{v}) &= \sum_{mn} B_{mn}^{(x)} N_m^{(k)}(\bar{u}) N_n^{(k)}(\bar{v}) \\ y(\bar{u},\bar{v}) &= \sum_{mn} B_{mn}^{(y)} N_m^{(k)}(\bar{u}) N_n^{(k)}(\bar{v}) \\ \xi_{1,2}^{A,D}(\bar{u},\bar{v}) &= \sum_{mn} \Gamma_{mn}^{(\tau)} N_m^{(k)}(\bar{u}) N_n^{(k)}(\bar{v}) \end{aligned} \tag{26}$$

where $\bar{u}$ and $\bar{v}$ are the parametric directions of the B-spline basis functions, $B_{mn}^{(x)}$ and $B_{mn}^{(y)}$ represent the location of each pre-defined control point P_{mn} along x and y axes, $\Gamma_{mn}^{(\tau)}$ is the assigned value of a particular lamination parameter at each P_{mn} and τ denotes different lamination parameters. The B-spline basis functions varying along $\bar{u}$ and $\bar{v}$ directions are $N_m^{(k)}(\bar{u})$ and $N_n^{(k)}(\bar{v})$, respectively and k represents the order ($k-1$ degree) of the piece-wise polynomial determined by a knot vector (Ξ). The optimal design is sought by adjusting the values of the lamination parameters ($\xi_{1,2}^{A,D}$) at the chosen control points along the plane of the plate.

2. *Globally convergent method of moving asymptote*

The optimization problem of VAT plates for maximizing the postbuckling performance using lamination parameters is formulated as,

$$\begin{aligned} \textbf{min} \quad & \epsilon_x(\Gamma_m^{(\tau)}) \quad or \quad W_{max}(\Gamma_m^{(\tau)})/h \\ \textbf{s.t.:} \quad & -1 \leqslant \Gamma_m^{(\tau)} \leqslant 1 \\ & g_i(\Gamma_m^{(\tau)}) \leqslant 0 \end{aligned} \tag{27}$$

where ϵ_x is the end shortening strain, W_{max} is the maximum postbuckling transverse displacement, h is the thickness of the laminate, $\Gamma_m^{(\tau)}$ is a vector form of lamination parameters at each P_{mn}, $g_i(\Gamma_m^{(\tau)})$ are nonlinear constraint functions that define relations between the four different lamination parameters, given by Eqns. 23-25.

In the proposed design framework, the globally convergent method of moving asymptote developed by Svanberg employs a successive convex approximation technique to solve the optimization problem. The objective functions and nonlinear constraints are replaced by a sequence of approximations (subproblems) based on gradient information, and these subproblems are created and solved iteratively until a desired convergence is achieved. Also, approximations of the objective function and nonlinear constraints in a local region are convex separable and conservative with respect to each design variable (lamination parameters). In the GCMMA method, the axial end-shortening strain/maximum transverse displacement and the nonlinear constraints in (27) are approximated as [36],

$$\bar{f}_i^{(\mu,\nu)}(\mathbf{\Gamma}) = \sum_{j=1}^{n} \left(\frac{p_{ij}^{(\mu,\nu)}}{\alpha_j^{(\mu)} - \Gamma_j} + \frac{q_{ij}^{(\mu,\nu)}}{\Gamma_j - \beta_j^{(\mu)}} \right) + r_i^{(\mu,\nu)} \tag{28}$$

where μ and ν respectively denote the indices of the "outer" and "inner" iterations, $\alpha_j^{(\mu)}$ and $\beta_j^{(\mu)}$ are the upper and lower moving asymptotes, respectively. For each design variable, the values of $p_{ij}^{(\mu,\nu)}$, $q_{ij}^{(\mu,\nu)}$ are associated with the positive and negative sensitivity, as well as the upper and lower moving asymptotes, respectively. The difference between the objective function and the approximation formula for the original design when each outer iteration begins is denoted by $r_i^{(\mu,\nu)}$. For the detailed expression of each variable in Eq. (28) refer to the work of Svanberg[37].

B. Second-Level Optimization

In the second level optimization process, the objective is to construct a realistic VAT layup that has lamination parameter distributions that closely match the optimal lamination distributions

obtained in the first-level optimization. The spatial variation of fiber angles for each VAT layer and the stacking sequence of the laminate needs to be determined. The problem of converting lamination parameters into VAT layups is quite complex [38] as there are no unique relationships between them. To accomplish this task, a genetic algorithm is employed to determine a VAT laminate configuration that closely matches the target lamination parameters. For each VAT layer, the nonlinear variation (NLV) of fiber orientations is defined based on a set of $M_1 \times N_1$ pre-selected control points in the plate domain. Lagrangian polynomials are used to interpolate the prescribed fiber angles at the control points and construct a nonlinear distribution of fiber angles, given by the following series form,

$$\theta(x,y) = \sum_{m=0}^{M_1-1} \sum_{n=0}^{N_1-1} T_{mn} \prod_{m \neq i} \left(\frac{x - x_i}{x_m - x_i}\right) \prod_{n \neq j} \left(\frac{y - y_j}{y_m - y_j}\right) \tag{29}$$

where the term T_{mn} is equal to the fiber angle at the control point (x_m, y_n). It is observed that three to five control points along each direction are usually sufficient to obtain converged fiber angle distribution results for a VAT panel. Furthermore, this fiber angle definition gives a continuous, smooth distribution for the fiber orientations, which are suitable for conversion into practical tow trajectories when manufacturing constraints are considered.

The fitness function is expressed as a mean value of the least square distance between the obtained lamination parameters and the target lamination parameters evaluated at a large number of points in the VAT plate. The optimization problem is formulated as,

$$\begin{aligned} \textbf{min} \quad & \Delta\xi = \frac{1}{N_p} \sum_j \Delta\xi_j \\ & \Delta\xi_j = \left[\sum_i^2 w_i^A \left(\xi_i^A - \tilde{\xi}_i^A\right)^2 + \sum_i^2 w_i^D \left(\xi_i^D - \tilde{\xi}_i^D\right)^2 \right]_{(j)} \\ & \xi_{1,2}^{A,D} \leftarrow \left[T_1^k, \cdots, T_n^k, \cdots, T_N^k\right] \\ \textbf{s.t.:} \quad & -\pi/2 \leqslant T_n^k \leqslant \pi/2 \end{aligned} \tag{30}$$

where T_n^k is the fiber angle at the control point for the k^{th} ply. w_i^A and w_i^D are the weights to distinguish the relative importance between $\xi_{1,2}^A$ and $\xi_{1,2}^D$. The term N_p is the total number of grid points and is chosen to be $1000 \sim 2000$ in total for a two dimensional variation.

VI. Results

This section presents the numerical results of the two-level optimization strategy for postbuckling design of VAT panels subjected to axial/bi-axial compression under different in-plane boundary conditions. Three cases of in-plane boundary conditions are considered in this work and the schematic diagram is shown in Fig. 1. The plate is subjected to uniform compression along the edges ($x = \pm\frac{a}{2} : u = \mp\frac{\Delta_x}{2}$) and in case A the transverse edges are free to move (stress free $\bar{N}_y = 0$), in case B the transverse edges are constrained ($v = 0$) and in case C the transverse edges are free to move and constrained to be straight. For the bi-axial case, the ratio of the compression loading N_y/N_x was chosen to be 0.2 and the schematic diagram of the loading is shown in Fig. 2. The postbuckling results are normalized with respect to the corresponding solutions of a homogeneous quasi-isotropic laminate. The equivalent Young's modulus E_{iso}, Poisson's ratio ν_{iso} and bending stiffness D_{iso} of a homogeneous quasi-isotropic (QI) laminate are given by [8],

$$D_{iso} = \frac{E_{iso}h^3}{12(1-\nu_{iso}^2)}, \quad \nu_{iso} = \frac{U_4}{U_1}, \quad E_{iso} = U_1(1-\nu_{iso}^2) \tag{31}$$

where U_1, U_2, U_4 are material invariants[33]. This normalization provides the designer with a useful measure to quantify the improvement of the optimal VAT laminate over a quasi-isotropic laminate.

At first, the accuracy of ANM in computing the postbuckling behavior of VAT plates under compression is analyzed and compared with ABAQUS FE results. Next, first level optimization was performed using GCMMA for obtaining optimal lamination parameter distributions that maximize the postbuckling performance of VAT panels under compression. Subsequently, the second level optimization was carried out using a genetic algorithm to convert the lamination parameters into realistic fiber angle distributions in the plane of the plate. Finally, the postbuckling performance of optimized VAT panel designs were compared with optimal straight fiber layups and the mechanics behind their improvement is discussed. The stress resultant distributions of an optimal VAT panel design corresponding to bi-axial loading was investigated in detail to explain the mechanics behind their improved postbuckling performance.

A. ANM results of VAT laminates

The accuracy and the range of validity of the postbuckling solution determined by the ANM approach is investigated for different in-plane boundary conditions as it is crucial for the optimization study of laminates. As a part of the numerical study, the ANM approach was applied to solve the postbuckling problem of symmetric VAT plates with linear fiber angle variation subjected to axial compression. The generalized differential-integral quadrature method implemented in MATLAB was then used to solve the linear problems obtained using ANM. The material properties for each lamina are given by E_1= 163 GPa, E_2=6.8 GPa, G_{12}= 3.4 GPa, ν_{12}= 0.28 with lamina thickness t=0.131 mm and number of laminae, n=16. The VAT plate with linear angle variation along the x direction is given by

$$\theta(x) = \phi + \frac{2(T_{10} - T_{00})}{a}|x| + T_{00} \tag{32}$$

where ϕ is the angle of rotation, T_{00} is the fiber orientation angle at the control point $x = 0, y = 0$, and T_{10} is the fiber orientation angle at the control point $x = \pm a/2, y = 0$ (see Fig. 1). The non-uniform grid distribution given by the Chebyshev-Gauss-Labotto points are used for the computation of weighting matrices and is given by

$$X_i = \frac{1}{2}[1 - cos(\frac{i-1}{N-1}\pi)], \quad i = 1, 2, ...N \tag{33}$$

where N is the number of grid points. The asymptotic expansions of the unknown load and displacement was limited to five terms in order to get reasonable accuracy over a finite load step size near the buckling point. The GDIQM was applied to solve five linear problems and the corresponding solutions were used to obtained the expansion coefficients of the asymptotic solutions. Padé approximants were then used in the asymptotic expansions of the ANM postbuckling solutions to improve the radius of convergence around the buckling point.

In order to validate the ANM results, finite element modeling of the VAT panels was carried out using ABAQUS. The S4 shell element was chosen for discretization of the VAT plate structure. To achieve good accuracy, a mesh size of 40×40 was selected for square VAT plates. Using the linear fiber angle definition, fiber orientation was evaluated at the centroid of each element. The material properties for elements were then defined using the fiber orientation information. Prior

to the buckling analysis, in-plane analysis of the VAT laminates under compression was carried out to compute the stress resultant distributions. The in-plane analysis results were then used in the buckling analysis for evaluating the critical buckling load coefficient. The postbuckling of VAT plates was then performed using buckling analysis results. The imperfection function required for nonlinear FE analysis was chosen to be the first buckling mode shape. The imperfection magnitude was taken to be one percent of the plate thickness and the arc length parameters required for Riks analysis were adapted to the particular VAT configuration analyzed. All plates considered in this study were considered to be simply supported.

The normalized postbuckling results of VAT plates with linear fiber angle variation for case A and case B obtained using ANM and FE approaches are shown in Figs. 3, 4 respectively. The results in Figs. 3 and 4 shows that the ANM results match the FE solutions over a finite radius around the buckling load for both the cases. Also, the postbuckling results computed using ANM exhibit a finite radius of convergence and the solution starts diverging beyond that point.

B. First level optimization-Optimal Lamination parameters

At the first level of optimization, optimal lamination parameter distributions for maximizing postbuckling performance of square VAT plates with all edges simply supported are presented. The optimal VAT laminate configuration which minimizes end-shortening strain or maximum transverse displacement may be different when the level of axial load (N_x) is changed. The length and width of the plate are $a = 0.5\ m$, $b = 0.5\ m$, respectively. In each optimization run, all the control points are uniformly distributed across the plate domain and uniform quadratic B-spline basis functions are used for constructing the variation of lamination parameters. Due to the symmetry of the buckling problem in terms of boundary conditions, geometry and loadings, the lamination parameter distribution is designed to be doubly symmetric, that is $\xi_{1,2}^{A,D}(x,y) = \xi_{1,2}^{A,D}(|x|,|y|)$. Hence, the lamination parameters are defined only at the control points on the quarter of the plate and symmetry conditions were then used to define the lamination parameter distributions in other quadrants of the plate model.

Initially end-shortening is minimized by finding optimal lamination parameters using a value

of N_x to be $2.5N_x^{iso}$. The end-shortening strain ϵ_x of the VAT panel is normalized with critical buckling strain ϵ_x^{iso}. Fig. 5 shows the convergence trends of the first-level optimization process, for the boundary conditions of case C, using different numbers (5×5; 7×7 and 9×9) of control points to construct the lamination parameter distributions. Correspondingly, the total number of design variables are 100 (25×4), 196 (49×4) and 324 (81×4). All control point distributions exhibit rapid convergence within a few iterations (around 15). It is observed that, with an increase of the number of control points, reduction of end-shortening axial strain is obtained. The curves for the 7×7 and 9×9 control points are nearly coincident when the optimization process converges. This also shows that the full design space can be achieved approximately by increasing the number of control points. It was observed that, for all cases, 7×7 control points for the B-splines to define the stiffness variation, is sufficient to yield converged postbuckling optimization results. The optimal variations (7×7 control points) of the four lamination parameters are plotted in Fig. 6, for case C. The contour plots of the lamination parameters in Fig. 6 exhibit smoothness without notable discontinuity and require fewer number of design variables compared to finite element based design approach [1]. Similarly, for the case A, case B and bi-axial loading, the optimal lamination parameter distributions results are shown in Figs. 7-9 respectively. For the cases C and A, the value of lamination parameter distributions $\xi_{1,2}^A$ (Fig 6 and 7) near the top and bottom regions of the VAT plate are closer to one and this leads to placement of 0^o fibers responsible for stiffening of the panel in the axial direction to take the compression load. For case B and bi-axial loading, the lamination parameters in the central region of the plate are $\xi_1^A \approx 0$ and $\xi_2^A \approx 1$ which corresponds to a combination of 0^o and 90^o plies. This lamination parameter distribution $\xi_{1,2}^A$ (Fig 8 and 9) leads to the improvement of axial and transverse membrane stiffness and enhances the postbuckling performance of VAT plates. Fig. 10 shows the prebuckling and postbuckling stress resultants distribution of the VAT panel corresponding to the optimal lamination parameter distribution of bi-axial loading. The $\bar{N}_x$ distribution in Figs. 10a, 10d shows redistribution of the applied axial compression load from the center towards the edges of the panel and leads to the improvement of the buckling and postbuckling performance. The $\bar{N}_y$ distribution (Fig. 10e) in the postbuckling regime indicates the presence of tensile stress state at the center of the panel which aids in resisting the

compression load in transverse direction and also contributes to the improvement of postbuckling stiffness of the plate.

C. Second level optimization-Optimal VAT layups

In the second level of optimization, conversion of the optimal lamination parameters into realistic variations of fiber orientation angles (or the tow trajectories) is performed. For a VAT laminate, the stacking sequence and spatial variation of fiber angles for each layer is required. A 3×3 control points grid is chosen on the quarter of each VAT design layer for defining the fiber angle variation in the plane of square plate thereby defining a quadratic variation in the fiber angle. The weights w_i^A, w_i^D were assumed to be identical for the lamination parameters $\xi_{1,2}^A$ and $\xi_{1,2}^D$, respectively. The stacking sequence is fixed to be a 16-layer symmetric laminate $[\pm\theta_1/\pm\theta_2/\pm\theta_3/\pm\theta_4]_S$ with four VAT design layers $(\theta_1(x,y), \theta_2(x,y), \theta_3(x,y), \theta_4(x,y))$ for the cases A, B and C. Figs. 11-13 show the spatially nonlinear varying fiber angle distributions of the optimal VAT layers for minimizing the end-shortening strain of the square VAT plate under different in-plane boundary conditions cases C, A and B, respectively. The VAT layups (Figs. 11, 12) of case C and A show 0^o fiber along the top and bottom edge of the panel that support the applied compression load and improves the overall stiffness of the laminate. The VAT layups (Fig. 13) in case B predominantly show fiber angles closer to 0^o across the panel to support the axial compression load. A VAT layup (Fig. 13b) in case B shows 90^o fiber angle at the center of the panel to support the compressive load in the transverse direction due to in-plane boundary condition ($v = 0$). For the bi-axial case, an anti-symmetrical stacking sequence with specially orthotropic properties ([B]=0, $A_{16} = A_{26} = 0$, $D_{16} = D_{26} = 0$) is considered. The stacking sequence was chosen to be a 32-layer anti-symmetric orthotropic laminate $[\pm\theta_1/\mp\theta_1/\pm\theta_2/\mp\theta_2/\pm\theta_3/\mp\theta_3/\pm\theta_4/\mp\theta_4]_{AS}$ with four VAT design layers $\theta_1(x,y), \theta_2(x,y), \theta_3(x,y), \theta_4(x,y)$ to suppress the deleterious effect of $D_{16} = D_{26} = 0$ on the postbuckling behavior. The optimal fiber angle distribution of the VAT layers that minimizes ϵ_x for the bi-axial case is shown in Fig. 14. Compared to other cases, the VAT layups (Fig. 14) for bi-axial loading show predominantly 0^o fiber around the central region of the panel and also the fiber angles along the top and bottom are not aligned completely with the loading direction. A VAT

layup (Fig. 14c) show 90^o fiber angle at the center of the panel to sustain the applied transverse compression load. The lamination parameter distribution for optimal VAT layup corresponding to bi-axial loading is shown in Fig. 15. The lamination parameter distribution shown in Fig. 15 matches up to 80 percent of the distribution shown in Fig. 9. This difference of the optimal VAT layup lamination parameter distribution with the optimal solution from the first level of optimization leads to a reduction in buckling and postbuckling performance. However, it is observed that 7 × 7 control points grid is sufficient to approximately match 95 percent of the optimal LP distribution shown in Fig. 9.

A direct GA search approach requires many (population size × the number of generations) postbuckling evaluation runs for the design of VAT plates. The computational effort increases considerably when many layers and control points are used. Nevertheless, this issue is avoided in the two-level optimization strategy. For the cases considered, less than 15 iterations are required to achieve the optimal lamination parameter distribution for the theoretically possible maximum postbuckling performance of VAT laminates. The subsequent process of retrieving realistic layups from the resultant lamination parameters requires little computational effort even when the design space is extended.

D. Optimization results

The postbuckling results comparing the performances of the optimal VAT laminate and straight fiber laminate design when normalized with a homogenous QI layup for the different in-plane boundary conditions (case C, case A, case B) are shown in Figs. 16-18 respectively. The end-shortening strain for a fixed axial compression load ($2.5N_{iso}$) gives a direct measure of the effective structural stiffness, which is a function of the pre-buckling and postbuckling stiffnesses of the laminate. Figs. 16-18 shows that the postbuckling performance of the optimal lamination parameters distributions attains the theoretical possible limit that can be achieved for the square VAT under compression. The optimal postbuckling design results for the VAT and straight fiber laminates are summarized in Table 1. For the optimal design of straight-fiber (constant stiffness) laminates, the layer angles for the laminate configuration are restricted to 5^o fiber angle increment from -90^o to 90^o. From Table

1, the layup $[\pm 45/0_6]_s$ gives the minimum end-shortening strain (ϵ_x) for both case A and case C. The performance of the optimal VAT layup is better than the optimal straight fiber design for all three cases studied and an improvement of 22% was observed for case C compared to the straight fiber laminate $[\pm 45/0_6]_s$. For case B, the VAT layup shown in Fig. 13 consists of fiber angles defined at control points closer to $0^o, 90^o$ and resembles the optimal straight fiber layup $[90_2/0_6]_s$ design. In addition, the improvement of 5.9% in postbuckling performance of optimal VAT layup over straight fiber design $[90_2/0_6]_s$ for case B is not as significant when compared to other cases. For the bi-axial loading case ($N_y/N_x = 0.2$) , the postbuckling results comparing the performances of the optimal VAT laminate and straight fiber laminate are shown in Fig. 19. The optimal straight fiber configuration that minimizes ϵ_x is given by the layup $[\pm 50/\mp 50/\pm 10/\mp 10/0_8]_{AS}$. The optimal VAT laminate exhibits a 8.8% improvement over the optimal straight fiber layup. The stress resultant distribution in the pre-buckling and post-buckling regime for the optimal VAT layups corresponding to bi-axial loading is shown in Fig. 20. The $\bar{N}_x$ distribution of VAT plate in the pre-buckling and post-buckling regime clearly shows the redistribution of the applied load towards the edge of the plate. The magnitude of $\bar{N}_y$ distribution in the postbuckling regime shows a tensile stress state which resists the applied compression load in the transverse direction and also aids in improving the postbuckling stiffness of the plate. For the optimal straight fiber layup of bi-axial loading, the prebuckling stress resultant distributions are found to be constant across the plane of the laminate and the postbuckling stress resultant distributions are shown in Fig. 21 which exhibits similar patterns to optimal VAT layup. As seen in Figs. 20, 21 the optimal VAT layup exhibits a greater degree of stress resultant redistribution compared with straight fiber layup and this is responsible for their superior buckling and postbuckling performance. The postbuckling design results of VAT panels for minimizing the maximum transverse displacement under axial compression is given in the supplementary material submitted along with this paper.

VII. Conclusion

In this work, a perturbation approach namely, the asymptotic numerical method was used to solve the postbuckling problem of VAT laminates under axial compression. The ANM approach was

Table 1 Optimum design for minimizing end-shortening strain ϵ_x

Cases	N_x/N_x^{iso}	Optimum layups	$\epsilon_x/\epsilon_x^{iso}$	Improvement (%)
case A, Str fib	2.5	$[\pm 45/0_6]_s$	2.91	-
case A, VAT	2.5	VAT Layup (Fig. 12)	2.64	10.4
case B, Str fib	2.5	$[90_2/0_6]_s$	2.17	-
case B, VAT	2.5	VAT Layup (Fig. 13)	2.05	5.9
case C, Str fib	2.5	$[\pm 45/0_6]_s$	2.71	-
case C, VAT	2.5	VAT Layup (Fig. 11)	2.22	22.1
Bi-axial, Str fib	2.5	$[\pm 50/\mp 50/\pm 10/\mp 10/0_8]_{AS}$	2.97	-
Bi-axial, VAT	2.5	VAT Layup (Fig. 14)	2.73	8.8

then successfully implemented using a generalized differential-integral quadrature method to solve the nonlinear postbuckling problem of VAT laminates in a computationally effective way suitable for optimization studies. The postbuckling results of VAT plates obtained using the ANM approach match FE solutions over a finite load step size around the buckling point for different in-plane boundary conditions. Usage of Padé approximation in the ANM approach further increased the range of convergence of the postbuckling solution of VAT plates.

A two-level optimization framework was applied to perform the postbuckling optimization of VAT composite plate under axial/bi-axial compression. Optimal lamination parameter distributions obtained using GCMMA gave insights into the in-plane stiffness distribution of VAT plates for maximizing the postbuckling performance under different in-plane boundary conditions. Furthermore, GA was applied to convert the optimal lamination parameters to nonlinear fiber distributions across the domain of the plate and provides an understanding on the placement of fiber paths to improve the postbuckling performance. The optimal laminate layups for straight fiber and VAT laminates were determined by minimizing the end-shortening strain in the postbuckling regime. From the optimization results, it is concluded that VAT laminates demonstrate improved buckling and postbuckling performance over constant stiffness laminates. In the future, the two-level optimization framework will be applied to design VAT plate and shell structures with stiffeners and cut-outs for improved postbuckling performance.

Acknowledgments

The authors wish to acknowledge EPSRC, Airbus and GKN for supporting this research under the project ABBSTRACT2 (EP/H025898/1) and also thank ACCIS Centre for Doctoral Training (EP/G036772/1) at Bristol. Paul M Weaver would like to thank the Science Foundation Ireland for funding VARICOMP under its Research Professor scheme

References

[1] Ijsselmuiden, S. T., Abdalla, M. M., Gurdal, Z., Optimization of variable-stiffness panels for maximum load using lamination parameters, *AIAA Journal*, Vol. 48, No. 1, 2010, pp. 134-43.

[2] Setoodeh, S., Abdalla, M. M., IJsselmuiden, S. T., and Gurdal, Z., Design of Variable-Stiffness Composite Panels for Maximum Buckling Load, *Composite Structures*, Vol. 87, No. 1, 2009, pp. 109-17.

[3] Wu, Z., Weaver, P. M., Raju, G., Kim, B., C., Buckling analysis and optimization of variable angle tow composite plates, *Thin-walled Structures*, Vol. 60, 2012, pp. 163-72.

[4] Falzon, B. G., Aliabadi, M. H., Buckling and postbuckling structures: Experimental, Analytical and Numerical studies, Imperial college press, 2008.

[5] Stein, M., Loads and deformation of rectangular plates with small initial curvature loaded in edge compression, *Journal of Applied Mechanics*, Vol. 18, 1959, pp. 143-51.

[6] Chandra, R., Raju, B., Postbuckling analysis of rectangular orthotropic plates, *International Journal of Mechanical Sciences*, Vol. 15, No. 1, 1973, pp. 81-97.

[7] Harris, G., The buckling and postbuckling behaviour of composite plates under biaxial loading, *International Journal of Mechanical Sciences*, Vol. 17, No. 3, 1975, pp. 187-202.

[8] Pandey, M. Sherbourne, A., Postbuckling behaviour of optimized rectangular composite laminates, *Composite Structures*, Vol. 23, No. 1, 1993, 27-38.

[9] Hui-Shen, S. and Jian-wu, Z., Perturbation analysis for the postbuckling of simply supported rectangular composite plates under uniaxial compression, *Applied Mathematics and Mechanics*, Vol. 9, 1988, pp. 793-804.

[10] Wu, Z., Raju, G., Weaver, P. M., Analysis and Design for the moderately deep postbuckling behaviour of composite plates, *Journal of Aircraft Structure*, 2016, http:/dx.doi.org/10.2514/1.C033875

[11] Rahman, T., Ijsselmuiden, S. T., Abdalla, M. M., Jansen, E. L., Postbuckling analysis of variable stiffness composite plates using a finite element based perturbation method, *International Journal of Structural Stability and Dynamics*, Vol. 11 , No. 4, 2011, pp. 735-53.

[12] Damil, N., Potier-Ferry, M., A new method to compute perturbed bifurcations: application to the buckling of imperfect elastic structures, *International Journal of Engineering Sciences*, Vol. 28, 1990, pp. 943-57.

[13] Azrar, L., Cochelin, B., Damil, N., Potier-Ferry, M., An asymptotic numerical method to compute the postbuckling behaviour of elastic plates and shells, *International Journal for Numerical Methods in Engineering*, Vol. 36, 1993, pp. 1251-77.

[14] Cochelin, B., Damil, N., Potier-Ferry, M., The asymptotic-numerical method: an efficient perturbation technique for nonlinear structural mechanics, *Revue Europenne des Elements*, Vol. 3, 1994, pp. 281-297.

[15] Ghiasi, H., Fayazbakhsh, K., Pasini, D., Lessard, L., Optimum stacking sequence design of composite materials Part II: Variable stiffness design, *Composite Structures*, Vol. 93, 2010, pp. 1-13.

[16] Wu, Z., Weaver, P. M., Raju, G., Postbuckling optimisation of variable angle tow composite plates, *Composite Structures*, Vol. 103, 2013, pp. 34-42.

[17] Henrichsen, S. R., Weaver, P. M., Lindgaard, E., Lund, E., Postbuckling optimization of composite structure using Koiter's method, *International Journal of Numerical Methods in Engineering*, Vol. 108, No. 8, 2016, pp. 902-940.

[18] Diaconu, C. G. and Weaver, P. M., Approximate solution and optimum design of compression-loaded postbuckled laminated composite plates, *AIAA Journal*, Vol. 43,2005, pp. 906-914.

[19] Diaconu, C. G. and Weaver, P. M., Postbuckling of long unsymmetrically laminated composite plates under axial compression,*International Journal of Solids and Structures*, Vol. 43 No. 22-23, 2006, pp. 6978-6997.

[20] Wu, Z., Raju, G., Weaver, P. M., Framework for the buckling optimization of variable angle tow composite plates, *AIAA Journal*, Vol. 53, No. 12, 2015, pp. 3788-3804.

[21] Grenestedt, J.L., Gudmundson, P., Lay-up optimization of composite material structures, *In Proc. IUTAM Symposium on Optimal design with Advanced Materials*, 1993, pp. 311-36, Amsterdam, The Netherlands: Elsevier Science.

[22] Wu, Z., Raju, G., Weaver P.M., Feasible region of lamination parameters for optimization of variable angle tow composite plates, *54rd AIAA/ASME/ASCE/AHS/ASC Structures, Structural Dynamics, and Materials Conference*, 2013.

[23] Koiter, W. T., On the stability of elastic equilibrium, *PhD thesis*, 1945, Techische School, Delft.

[24] Budiansky, B., Theory of buckling and postbuckling behavior of elastic structures, *Advances in Applied Mechanics*, Vol. 14, 1975, pp. 1-65.

[25] Washizu, K., Variational methods in elasticity and plasticity, Second Edition-Pergamon Press, 1975.

[26] Raju, G., Wu, Z., Kim, B. C., Weaver, P. M., Pre-buckling and buckling analysis of variable angle tow plates with general boundary conditions, *Composite Structures*, Vol. 94, No. 9, 2012, pp. 2961-70.

[27] Raju, G., Wu, Z., Weaver, P. M., Postbuckling analysis of variable angle tow plates using differential quadrature method, *Composite Structures*, Vol. 106, 2013, pp. 74-84.

[28] Shu C. Differential quadrature and its application in engineering, London: Springer-Verlag, 2000.

[29] Shu, C., Chew, Y. T., Richards, B. E., Generalized differential and integral quadrature and their application to solve boundary layer equations, *International journal for numerical methods in fluids*, Vol. 21, No. 9,pp. 723-733.

[30] White, S., Raju, G., Weaver, P. M., Initial postbuckling of variable stiffness curved panels, *Journal of the Mechanics and Physics of Solids*, Vol. 71, 2014, pp. 132-55.

[31] Penrose, R., A generalized inverse for matrices, *In Proc. Cambridge Philos. Soc*, Vol. 51, No. 3, 1955, pp. 406-413.

[32] Tsai, S. W., Hahn, H. T., Introduction to composite materials, Stanford, CT: Technomic Publishing Co., Inc, 1980.

[33] Jones, R., M., Mechanics of Composite materials, CRC press, 2nd Revised edition, 1998.

[34] Bloomfield, M., Diaconu, C., Weaver, P.M., On feasible regions of lamination parameters for lay-up optimization of laminated composites, *Proceedings of the Royal Society A: Mathematical, Physical and Engineering Sciences*, Vol. 465, 2009, pp. 1123-43.

[35] Setoodeh, S., Abdalla, M.M, Gurdal, Z., Approximate feasible regions for lamination parameters, *AIAA Journal*, Vol. 2, 2006, pp. 814-22.

[36] Svanberg, K., MMA and GCMMA versions September 2007.

[37] Svanberg, K., The method of moving asymptotes- a new method for structural optimization, *International Journal of Numerical methods in Engineering*, Vol. 24, 359-73, 1987.

[38] Van Campen, J. M. J. F., Kassapoglou, C., Gurdal, Z., Generating realistic laminate fiber angle distributions for optimal variable stiffness laminates, *Composites Part B: Engineering*, Vol. 43, No. 2, 2012, pp. 354-60.

VIII. Appendix

The ANM approach converts the postbuckling problem of VAT plates into a set of linear problems and the GDIQM numerical formulation of the different order problems are presented as follows.

A. Zeroth order analysis of VAT laminates

The zeroth order analysis corresponds to the prebuckling problem of VAT plates and the GDIQM implementation written in matrix form is given by,

$$\begin{bmatrix} K_{uu} & K_{uv} \\ K_{vu} & K_{vv} \end{bmatrix} \begin{Bmatrix} u_0 \\ v_0 \end{Bmatrix} = \begin{Bmatrix} F_{u0} \\ F_{v0} \end{Bmatrix} \tag{34}$$

$$\begin{aligned} K_{uu} &= \int_{\Omega} \frac{\partial^{'}}{\partial x} A_{11} \frac{\partial}{\partial x} + \frac{\partial^{'}}{\partial y} A_{66} \frac{\partial}{\partial y} d\Omega = A_{11} \mathbf{T}^{x^{'}} \mathbf{M} \mathbf{T}^{x} + A_{66} \mathbf{T}^{y^{'}} \mathbf{M} \mathbf{T}^{y} \\ K_{uv} = K_{vu} &= \int_{\Omega} \frac{\partial^{'}}{\partial x} A_{12} \frac{\partial}{\partial y} + \frac{\partial^{'}}{\partial y} A_{66} \frac{\partial}{\partial x} d\Omega = A_{12} \mathbf{T}^{x^{'}} \mathbf{M} \mathbf{T}^{y} + A_{66} \mathbf{T}^{y^{'}} \mathbf{M} \mathbf{T}^{x} \\ K_{vv} &= \int_{\Omega} \frac{\partial^{'}}{\partial y} A_{22} \frac{\partial}{\partial y} + \frac{\partial^{'}}{\partial x} A_{66} \frac{\partial}{\partial x} d\Omega = A_{22} \mathbf{T}^{y^{'}} \mathbf{M} \mathbf{T}^{y} + A_{66} \mathbf{T}^{x^{'}} \mathbf{M} \mathbf{T}^{x} \end{aligned} \tag{35}$$

where $U_0 = \begin{Bmatrix} u_0 \\ v_0 \end{Bmatrix}$ represents the zeroth order solution and F_{u0}, F_{v0} represents the forces applied along the x and y directions. The terms $\mathbf{T}^{x}, \mathbf{T}^{y}$ represent the first-order derivative matrix operator and their transposes are given by $\mathbf{T}^{x^{'}}, \mathbf{T}^{y^{'}}$ respectively. The term $\mathbf{M}$ represent the integral quadrature matrix operator over a surface area Ω.

B. First order analysis of VAT laminates

The first order analysis which corresponds to the buckling problem of VAT plates is governed by the bending behavior of the plates. The eigen value buckling problem in standard matrix form is

$$[K_{ww} - \lambda_c K_g] w = 0 \tag{36}$$

$$
\begin{aligned}
K_{ww} &= \int_{\Omega} \frac{\partial^{2^{'}}}{\partial x^2} D_{11} \frac{\partial^2}{\partial x^2} + \frac{\partial^{2^{'}}}{\partial y^2} D_{22} \frac{\partial^2}{\partial y^2} + 2\frac{\partial^{2^{'}}}{\partial x^2} D_{12} \frac{\partial^2}{\partial y^2} + 4\frac{\partial^{2^{'}}}{\partial x \partial y} D_{66} \frac{\partial^2}{\partial x \partial y} \\
&\qquad + 4\frac{\partial^{2^{'}}}{\partial x^2} D_{16} \frac{\partial^2}{\partial x \partial y} + 4\frac{\partial^{2^{'}}}{\partial y^2} D_{26} \frac{\partial^2}{\partial x \partial y} d\Omega \\
&= D_{11}\mathbf{T}^{xx^{'}}\mathbf{M}\mathbf{T}^{xx} + D_{22}\mathbf{T}^{yy^{'}}\mathbf{M}\mathbf{T}^{yy} + 2D_{12}\mathbf{T}^{xx^{'}}\mathbf{M}\mathbf{T}^{yy} + 4D_{66}\mathbf{T}^{xy^{'}}\mathbf{M}\mathbf{T}^{xy} \\
&\qquad + 4D_{16}\mathbf{T}^{xx^{'}}\mathbf{M}\mathbf{T}^{xy} + 4D_{26}\mathbf{T}^{yy^{'}}\mathbf{M}\mathbf{T}^{xy} \\
K_g &= \int_{\Omega} \frac{\partial^{'}}{\partial x} \bar{N}_{0x} \frac{\partial^{'}}{\partial x} + \frac{\partial^{'}}{\partial y} \bar{N}_{0y} \frac{\partial^{'}}{\partial y} + 2\frac{\partial^{'}}{\partial x} \bar{N}_{0xy} \frac{\partial^{'}}{\partial y} d\Omega \\
&= \bar{N}_{0x}\mathbf{T}^{x^{'}}\mathbf{M}\mathbf{T}^{x} + \bar{N}_{0y}\mathbf{T}^{y^{'}}\mathbf{M}\mathbf{T}^{y} + 2\bar{N}_{0xy}\mathbf{T}^{x^{'}}\mathbf{M}\mathbf{T}^{y}
\end{aligned}
\tag{37}
$$

where K_g represents the geometric stiffness matrix and $\bar{N}_{0x}, \bar{N}_{0y}, \bar{N}_{0xy}$ represents the prebuckling stress resultants. The terms $\mathbf{T}^{xx}, \mathbf{T}^{yy}, \mathbf{T}^{xy}$ represent the second-order derivative matrix operators.

C. Second order analysis of VAT laminates

The second order analysis corresponds to computation of the postbuckling displacement field

$$
\begin{bmatrix} K_{uu} & K_{uv} \\ K_{vu} & K_{vv} \end{bmatrix} \begin{Bmatrix} u_2 \\ v_2 \end{Bmatrix} = \begin{Bmatrix} F_{u2} \\ F_{v2} \end{Bmatrix} \tag{38}
$$

$$
\begin{aligned}
F_{u2} &= -\frac{1}{2} \int_{\Omega} \frac{\partial^{'}}{\partial x} A_{11} \frac{\partial w_1}{\partial x}^2 + \frac{\partial^{'}}{\partial x} A_{12} \frac{\partial w_1}{\partial y}^2 + \frac{\partial^{'}}{\partial x} A_{66} (\frac{\partial w_1}{\partial x}\frac{\partial w_1}{\partial y} + \frac{\partial w_1}{\partial y}\frac{\partial w_1}{\partial x}) d\Omega \\
&= -\frac{1}{2}(A_{11}\mathbf{T}^{x^{'}}\mathbf{M}(\mathbf{T}^{x}w_1)^2 + A_{12}\mathbf{T}^{x^{'}}\mathbf{M}(\mathbf{T}^{y}w_1)^2 + A_{66}\mathbf{T}^{x^{'}}\mathbf{M}(\mathbf{T}^{x}w_1\mathbf{T}^{y}w_1 + \mathbf{T}^{y}w_1\mathbf{T}^{x}w_1)) \\
F_{v2} &= -\frac{1}{2} \int_{\Omega} \frac{\partial^{'}}{\partial y} A_{12} \frac{\partial w_1}{\partial x}^2 + \frac{\partial^{'}}{\partial y} A_{22} \frac{\partial w_1}{\partial y}^2 + \frac{\partial^{'}}{\partial y} A_{66} (\frac{\partial w_1}{\partial x}\frac{\partial w_1}{\partial y} + \frac{\partial w_1}{\partial y}\frac{\partial w_1}{\partial x}) d\Omega \\
&= -\frac{1}{2}(A_{12}\mathbf{T}^{y^{'}}\mathbf{M}(\mathbf{T}^{x}w_1)^2 + A_{22}\mathbf{T}^{y^{'}}\mathbf{M}(\mathbf{T}^{y}w_1)^2 + A_{66}\mathbf{T}^{y^{'}}\mathbf{M}(\mathbf{T}^{x}w_1\mathbf{T}^{y}w_1 + \mathbf{T}^{y}w_1\mathbf{T}^{x}w_1))
\end{aligned}
\tag{39}
$$

where $U_2 = \begin{Bmatrix} u_2 \\ v_2 \end{Bmatrix}$ is the second order displacement field. The second order stress resultant $\bar{N}_{\alpha\beta}$ is obtained by the constitutive relationship

$$
\begin{Bmatrix} \bar{N}_{2x} \\ \bar{N}_{2y} \\ \bar{N}_{2y} \end{Bmatrix} = \begin{bmatrix} A_{11} & A_{12} & A_{16} \\ A_{12} & A_{22} & A_{26} \\ A_{16} & A_{26} & A_{66} \end{bmatrix} \begin{Bmatrix} u_{2,x} + \frac{1}{2}w_{1,x}^2 \\ v_{2,y} + \frac{1}{2}w_{1,y}^2 \\ u_{2,y} + v_{2,x} + w_{1,x}w_{1,y} \end{Bmatrix} \tag{40}
$$

D. Third order analysis of VAT laminates

The third order displacement field w_3 is obtained by solving

$$\begin{bmatrix} K_{ww} - \lambda_c K_g & G^* \\ G^{*t} & 0 \end{bmatrix} \begin{Bmatrix} w_3 \\ \mu \end{Bmatrix} = \begin{Bmatrix} F_{w3} \\ 0 \end{Bmatrix} \tag{41}$$

where $G = [K_{ww}]w_1$ and μ is a Lagrange multiplier. The force vector F_{w3} is computed by the expression given by

$$\begin{aligned} F_{w3} = \int_\Omega & -\frac{\partial'}{\partial x}\left[(\bar{N}_{0x}C(2) + \bar{N}_{2x})\frac{\partial w_1}{\partial x} + (\bar{N}_{0xy}C(2) + \bar{N}_{2xy})\frac{\partial w_1}{\partial y}\right] \\ & - \frac{\partial'}{\partial y}\left[(\bar{N}_{0xy}C(2) + \bar{N}_{2xy})\frac{\partial w_1}{\partial x} + (\bar{N}_{0y}C(2) + \bar{N}_{2y})\frac{\partial w_1}{\partial y}\right] d\Omega \\ = -[&(\bar{N}_{0x}C(2) + \bar{N}_{2x})\mathbf{T}^{x'}\mathbf{M}(\mathbf{T}^x w_1) + (\bar{N}_{0xy}C(2) + \bar{N}_{2xy})\mathbf{T}^{x'}\mathbf{M}(\mathbf{T}^y w_1) \\ & + (\bar{N}_{0xy}C(2) + \bar{N}_{2xy})\mathbf{T}^{y'}\mathbf{M}(\mathbf{T}^x w_1) + (\bar{N}_{0y}C(2) + \bar{N}_{2y})\mathbf{T}^{y'}\mathbf{M}(\mathbf{T}^y w_1)] \end{aligned} \tag{42}$$

The constant $C(2)$ is computed by

$$C(2) = \frac{\int_\Omega \bar{N}_{\alpha\beta}(2) w_{1,\alpha} w_{1,\beta} d\Omega}{\int_\Omega \bar{N}_{\alpha\beta}(0) w_{1,\alpha} w_{1,\beta} d\Omega} \tag{43}$$

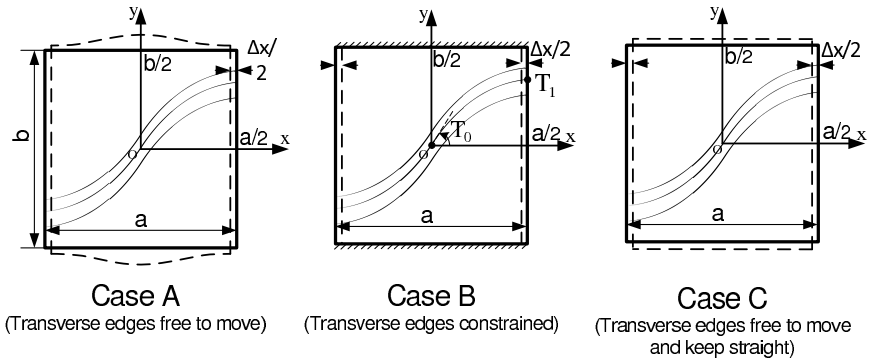

Fig. 1 Geometry and boundary conditions.

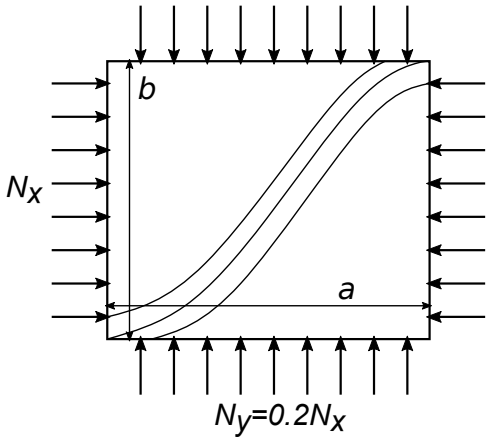

Fig. 2 Bi-axial loading conditions.

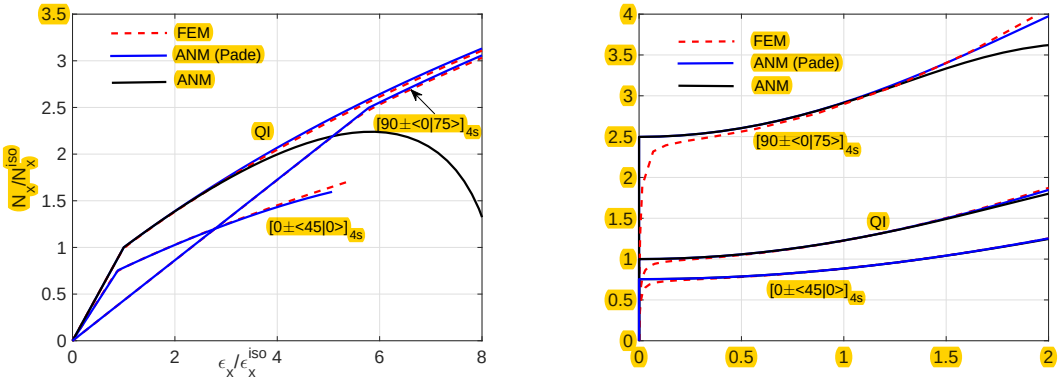

Fig. 3 ANM and FE solutions of a square simply-supported plate subjected to case A (a) Normalized axial load N_x/N_x^{iso} versus Normalized axial strain $\epsilon_x/\epsilon_x^{iso}$ (b) Normalized axial load N_x/N_x^{iso} versus Normalized maximum transverse displacement W/h.

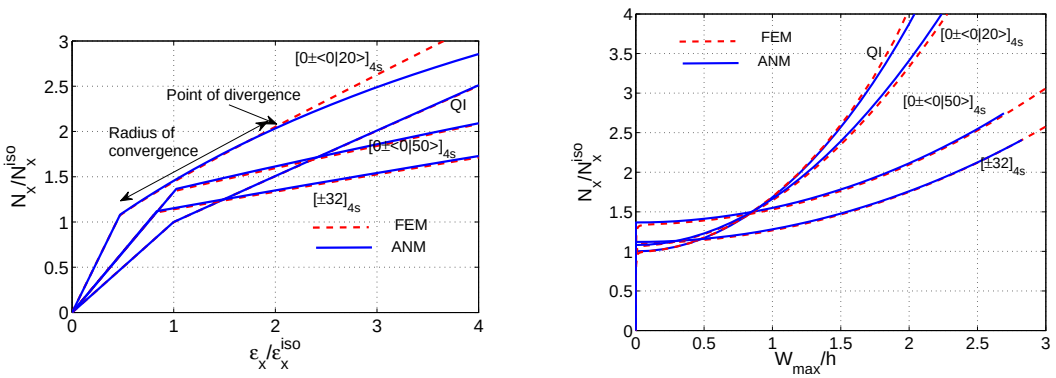

(a) (b)

Fig. 4 ANM and FE solutions of a square simply-supported plate subjected to case B (a) Normalized axial load N_x/N_x^{iso} versus Normalized axial strain $\epsilon_x/\epsilon_x^{iso}$ (b) Normalized axial load N_x/N_x^{iso} versus Normalized maximum transverse displacement W/h

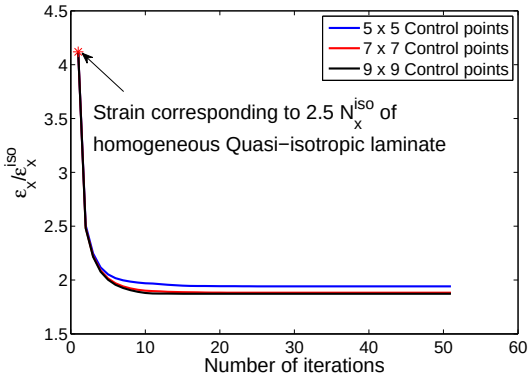

Fig. 5 Convergence trends of the first level optimization process using different number of control points for constructing the B-spline form variation of lamination parameters (case C).

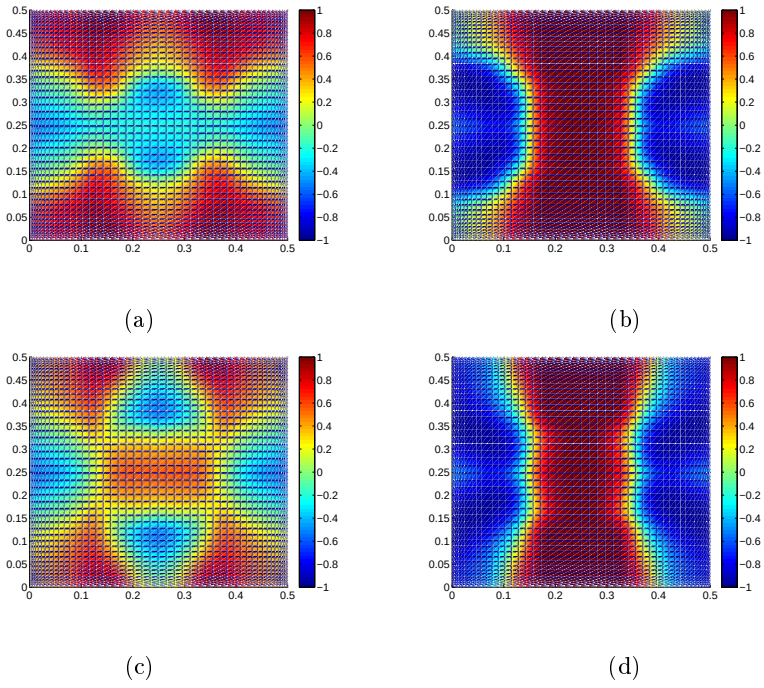

(a) (b)

(c) (d)

Fig. 6 Optimal lamination parameter distribution for minimizing ϵ_x of a square simply-supported plate subjected to case C (a)ξ_1^A (b)ξ_2^A (c)ξ_1^D (d)ξ_2^D

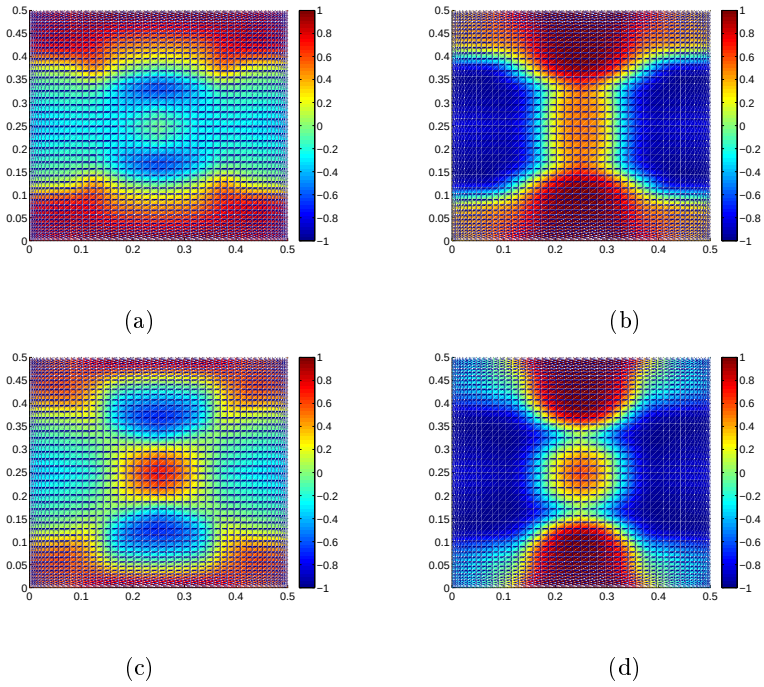

(a) (b)

(c) (d)

Fig. 7 Optimal lamination parameter distribution for minimizing ϵ_x of a square simply-supported plate subjected to case A (a)ξ_1^A (b)ξ_2^A (c)ξ_1^D (d)ξ_2^D

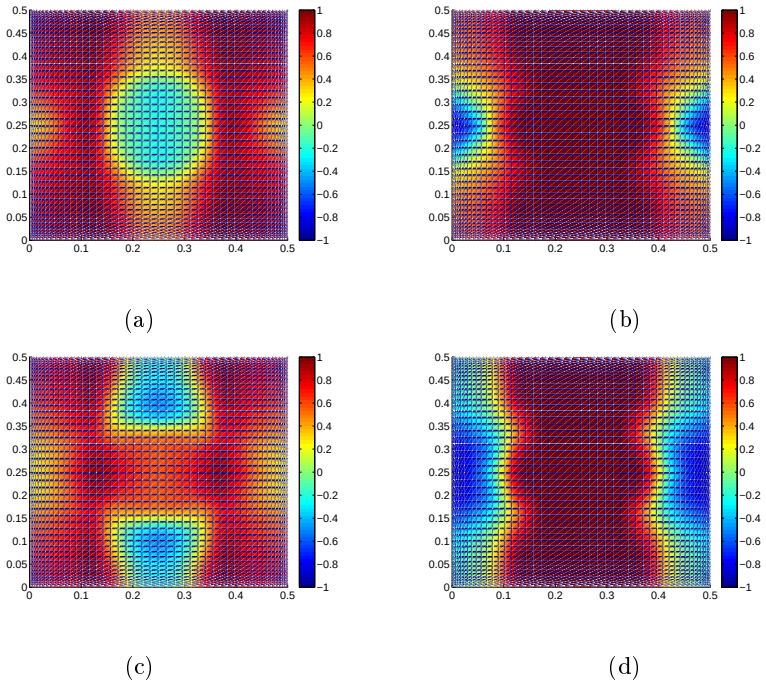

(a) (b)

(c) (d)

Fig. 8 Optimal lamination parameter distribution for minimizing ϵ_x of a square simply-supported plate subjected to case B (a)ξ_1^A (b)ξ_2^A (c)ξ_1^D (d)ξ_2^D

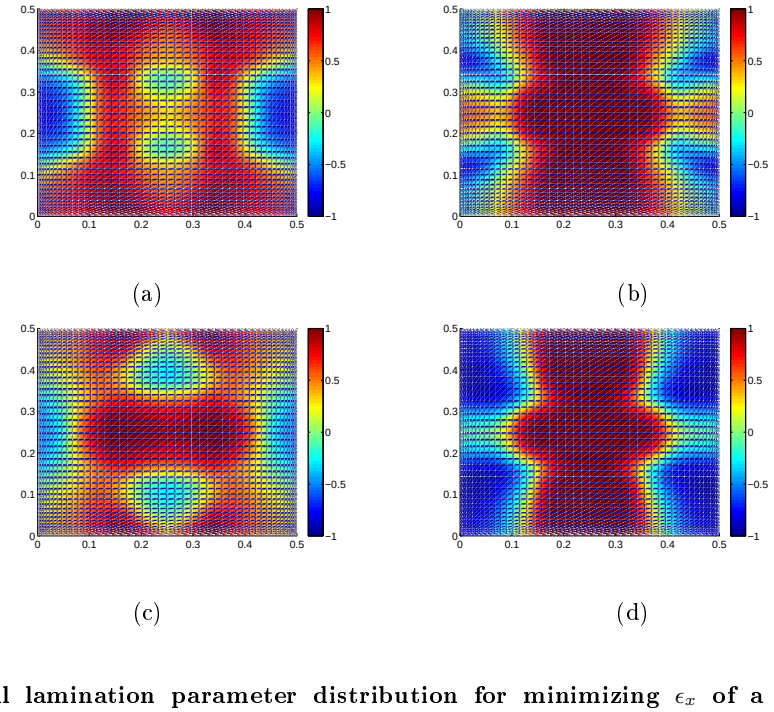

(a) (b)

(c) (d)

Fig. 9 Optimal lamination parameter distribution for minimizing ϵ_x of a square simply-supported plate subjected to bi-axial loading $N_y/N_x = 0.2$ (a)ξ_1^A (b)ξ_2^A (c)ξ_1^D (d)ξ_2^D

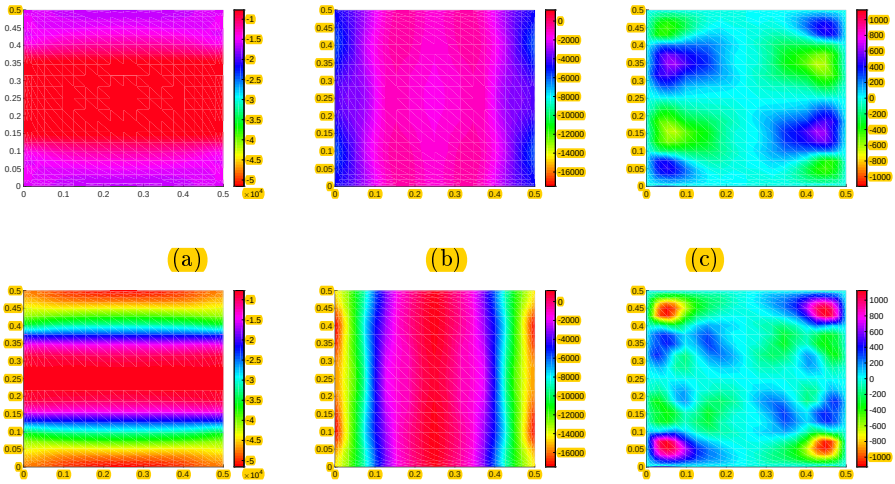

Fig. 10 Stress resultant distributions for the optimal lamination parameter corresponding to bi-axial loading $N_y/N_x = 0.2$ (a)$\bar{N}_x$ (Prebuckling state) (b)$\bar{N}_y$ (Prebuckling state) (c)$\bar{N}_{xy}$ (Prebuckling state) (d)$\bar{N}_x$ (Postbuckling state at 2.5 N^x_{iso}) (e)$\bar{N}_y$ (Postbuckling state at 2.5 N^x_{iso}) (f)$\bar{N}_{xy}$ (Postbuckling state at 2.5 N^x_{iso})

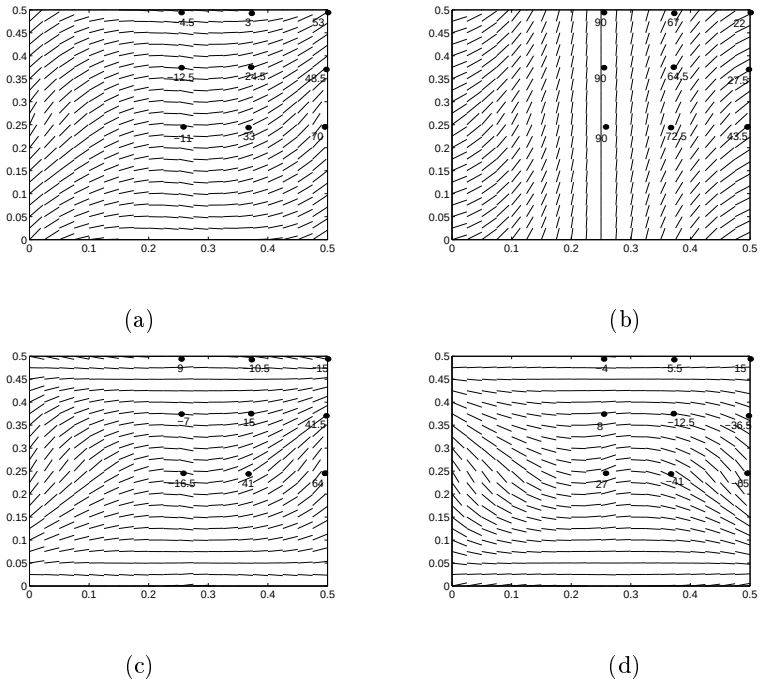

Fig. 11 The optimum nonlinear variation (3×3 control points for each layer) of fiber-orientation distribution for minimizing ϵ_x of the square simply supported VAT plate design for case C (a) VAT layer1 (b) VAT layer2 (c) VAT layer3 (d) VAT layer4

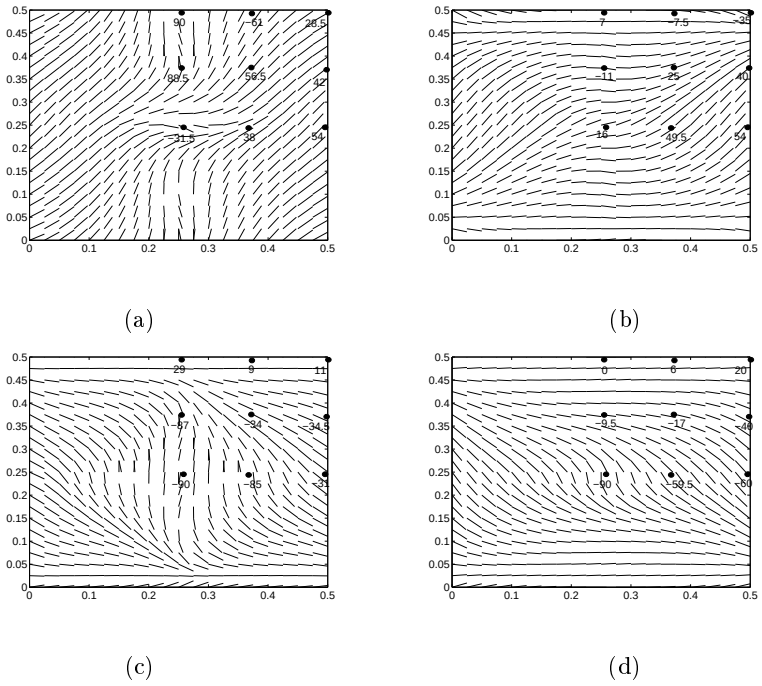

Fig. 12 The optimum nonlinear variation (3×3 control points for each layer) of fiber-orientation distribution for minimizing ϵ_x of the square simply supported VAT plate design for case A (a) VAT layer1 (b) VAT layer2 (c) VAT layer3 (d) VAT layer4

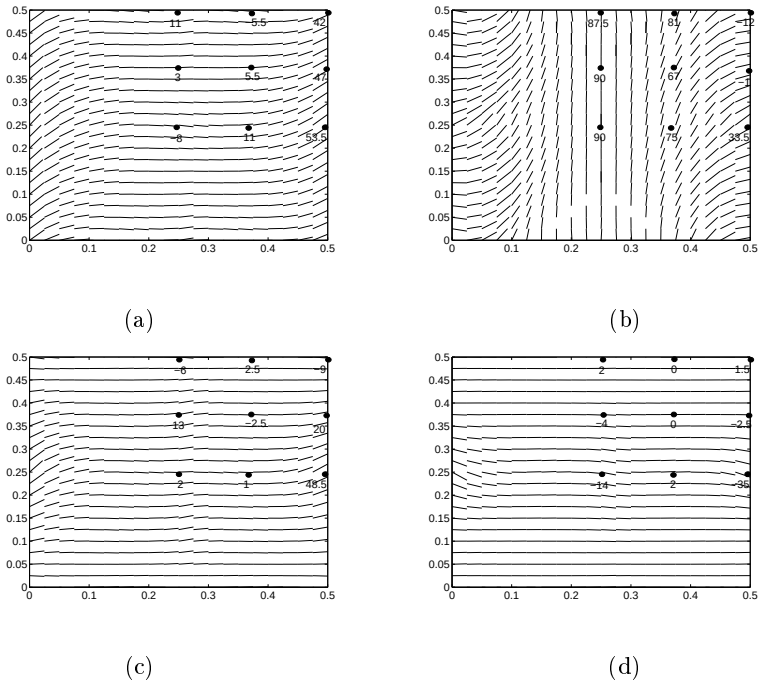

(a) (b)

(c) (d)

Fig. 13 The optimum nonlinear variation (3×3 control points for each layer) of fiber-orientation distribution for minimizing ϵ_x of the square simply supported VAT plate design for case B (a) VAT layer1 (b) VAT layer2 (c) VAT layer3 (d) VAT layer4

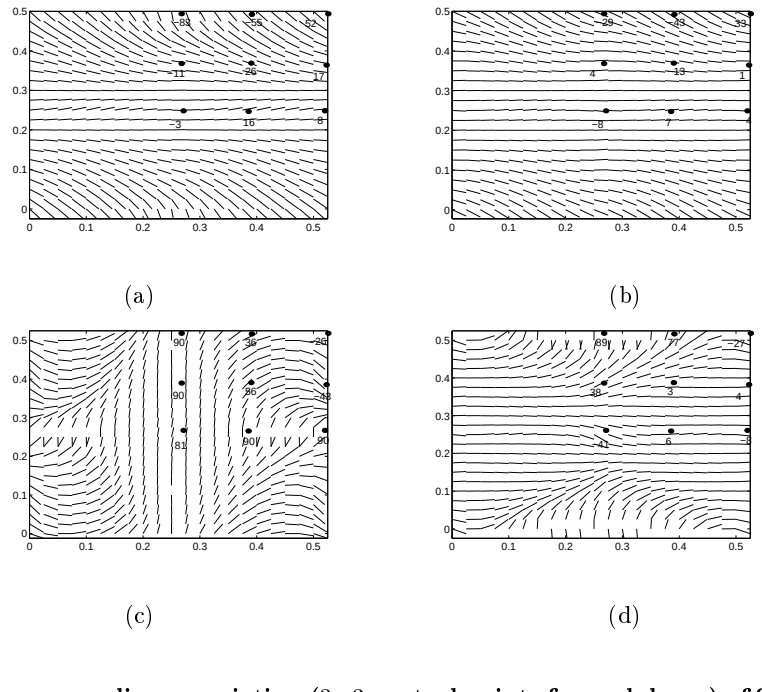

(a) (b)

(c) (d)

Fig. 14 The optimum nonlinear variation (3×3 control points for each layer) of fiber-orientation distribution for minimizing ϵ_x of the square simply supported VAT plate design for bi-axial loading $N_y/N_x = 0.2$ (a) VAT layer1 (b) VAT layer2 (c) VAT layer3 (d) VAT layer4

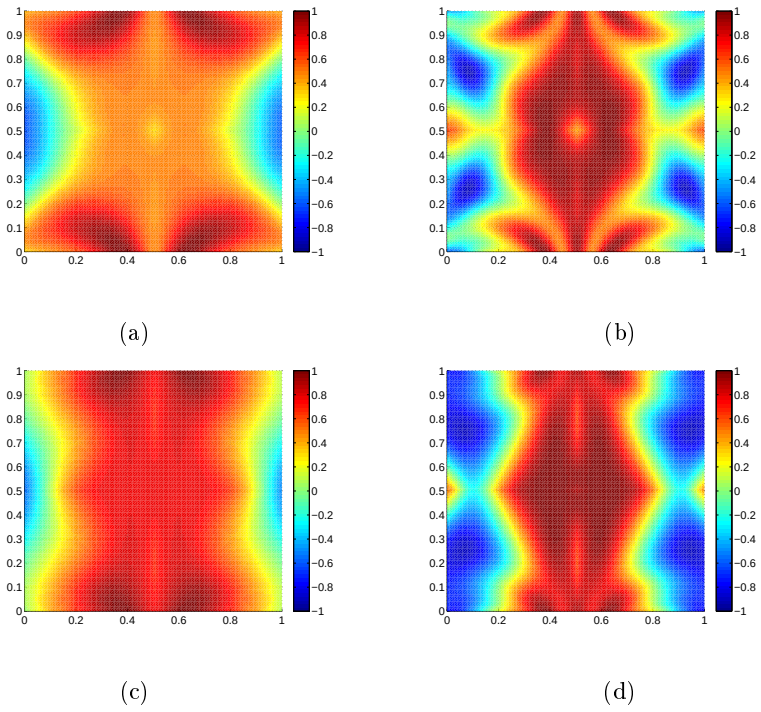

Fig. 15 Lamination parameter distribution for optimal VAT layup (Fig 9) corresponding to bi-axial loading $N_y/N_x = 0.2$ (a)ξ_1^A (b)ξ_2^A (c)ξ_1^D (d)ξ_2^D

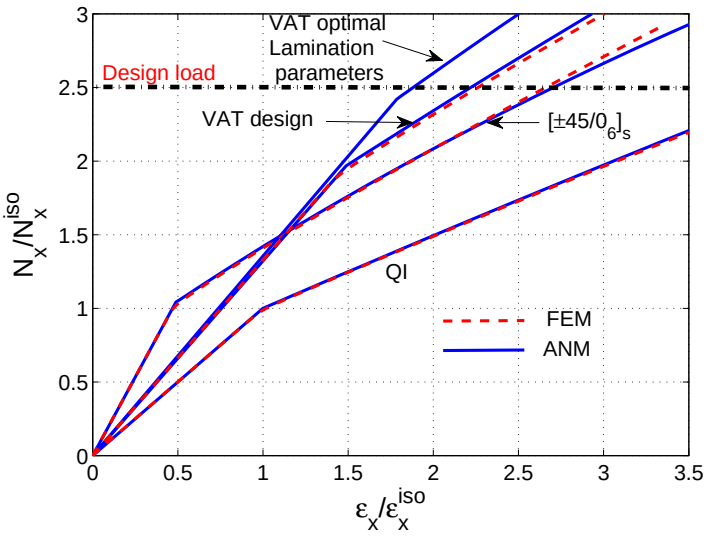

Fig. 16 ANM and FE solutions of optimal straight fiber and VAT laminate designs for case C: Normalized axial load N_x/N_x^{iso} versus Normalised axial strain $\epsilon_x/\epsilon_x^{iso}$

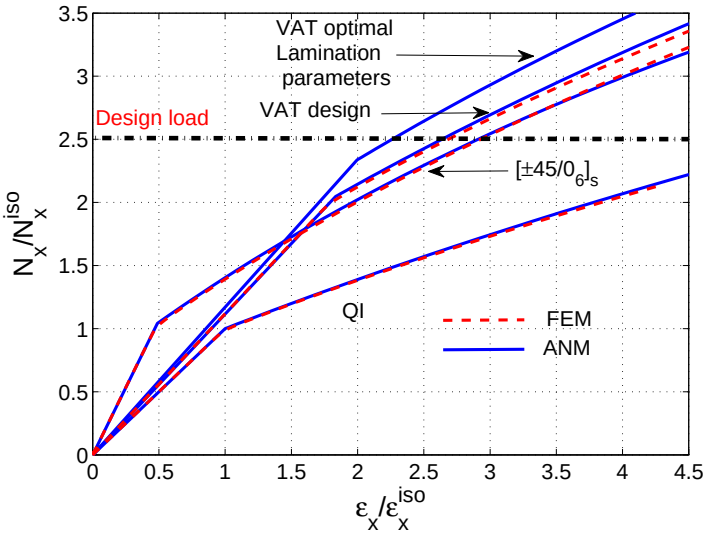

Fig. 17 ANM and FE solutions of optimal straight fiber and VAT laminate designs for case A: Normalized axial load N_x/N_x^{iso} versus Normalised axial strain $\epsilon_x/\epsilon_x^{iso}$

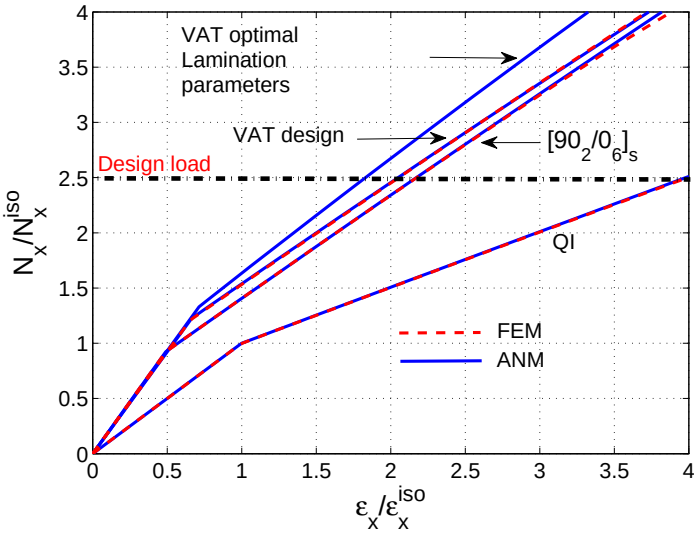

Fig. 18 ANM and FE solutions of optimal straight fiber and VAT laminate designs for case B: Normalized axial load N_x/N_x^{iso} versus Normalised axial strain $\epsilon_x/\epsilon_x^{iso}$

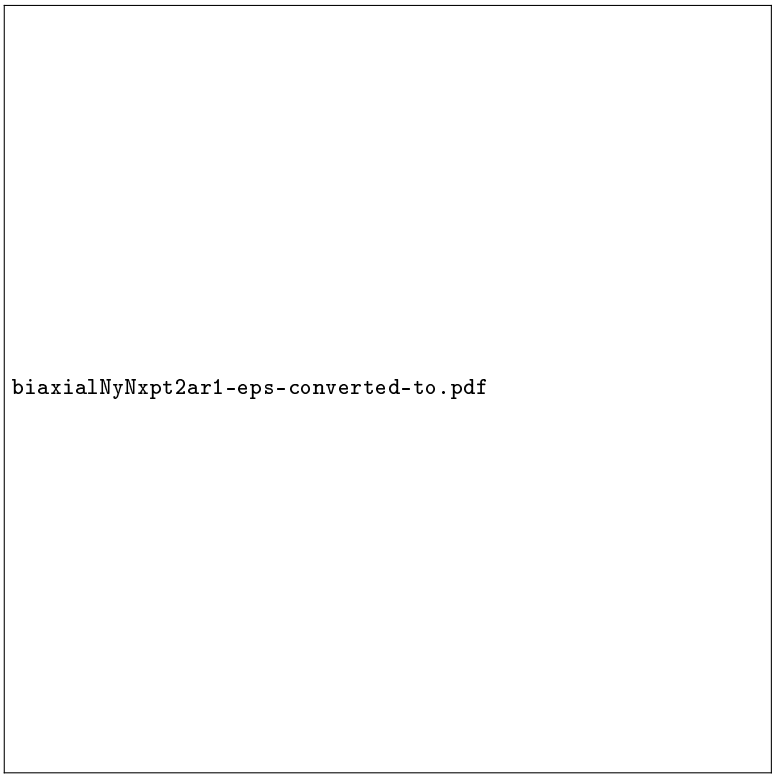

Fig. 19 ANM and FE solutions of optimal straight fiber and VAT laminate designs for bi-axial loading $N_y/N_x = 0.2$: Normalized axial load N_x/N_x^{iso} versus Normalised axial strain $\epsilon_x/\epsilon_x^{iso}$

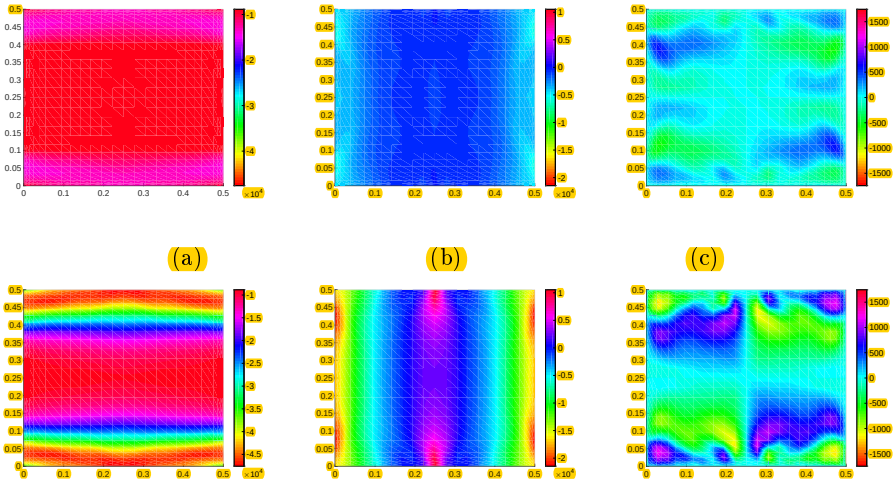

Fig. 20 Stress resultant distributions for the optimal VAT design corresponding to bi-axial loading $N_y/N_x = 0.2$ (a)$\bar{N}_x$ (Prebuckling state) (b)$\bar{N}_y$ (Prebuckling state) (c)$\bar{N}_{xy}$ (Prebuckling state) (d)$\bar{N}_x$ (Postbuckling state at 2.5 N_{iso}^x) (e)$\bar{N}_y$ (Postbuckling state at 2.5 N_{iso}^x) (f)$\bar{N}_{xy}$ (Postbuckling state at 2.5 N_{iso}^x)

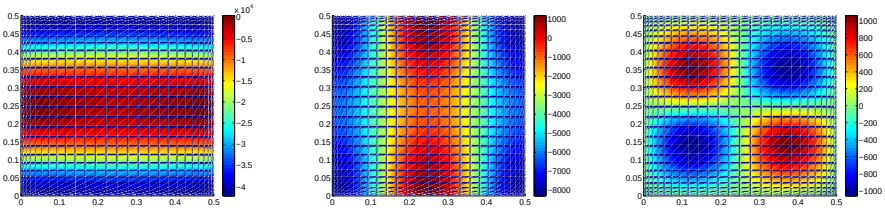

(a) (b) (c)

Fig. 21 Stress resultant distributions for the optimal straight fiber design corresponding to bi-axial loading $N_y/N_x = 0.2$ (a)$\bar{N}_x$ (Postbuckling state at 2.5 N^x_{iso}) (b)$\bar{N}_y$ (Postbuckling state at 2.5 N^x_{iso}) (c)$\bar{N}_{xy}$ (Postbuckling state at 2.5 N^x_{iso})